Universitat Politècnica de València

Instituto CMT - Motores Térmicos

A COMPUTATIONAL FLUID DYNAMICS ANALYSIS OF VORTICITY REDUCTION FOR TURBOCHARGED INTERNAL COMBUSTION ENGINES

DEGREE THESIS

Author: Daniel Wilczynski

Tutor: Antonio Gil Megías, Ph.D.

Cotutor: Pau Raga Nieto

AEROSPACE ENGINEERING DEGREE

JET ENGINES SPECIALTY

4th YEAR, JULY 2017

Acknowledgements

I would very much like to express my sincere gratitude towards my supervisors in the development of this degree thesis, i.e. Antonio Gil Megías, Ph.D. and Pau Raga Nieto, for their complete and constant assistance in all the stages of the project.

Apart from it, I would like to thank all the members of the Investigation Centre CMT - Thermal Engines and Machines, especially Pedro Manuel Quintero Igeño, for all the help provided during my learning of the Star CCM+ software, as well as during solving all the doubts and issues pertaining to the CFD analysis.

Thanks to their guidance and support I have been able to learn the basics related to the CFD systems tools and to acquire skills that will be, with no doubt, indispensable in all the future projects in the field of the aerospace engineering.

Abstract

The degree thesis developed in the document hereof, aims at performing a Computational Fluid Dynamics study of a swirl flow inside a duct, implementing all sorts of designs in order to mitigate the swirl as much as possible. Another primordial aspect is the pressure drop control between the inlet and the outlet, that should also be attempted to be as low as it can get.

The software used as the tool of the project is Star CCM+, one of the most important CFD programs in all of the fluid mechanics. Prior to the explanation of the designs, all the crucial aspects of a CFD analysis shall be presented and meticulously illustrated, in order to allow the reader to get more familiar with the processes used. It will cover all the three main stages of the simulation, i.e. preprocess, solver and the postprocess, and the most important steps in each of them. Apart from it, a quick view at the main methodology that could be used to resolve the swirl problem, will be presented.

In the beginning of the project, a former CAD design from previous work was delivered, based on an internal stator geometry. It was immediately determined that the geometry provided was not effective as a swirl reduction method and that it must be either much improved or substituted. For this purpose, 29 original and different designs have been created, and then implemented successfully. One of them was a considerable enhancement of the stator-given geometry, while the other 28 managed to reduce in a greater or less extent, the swirl that appeared in the duct. As it will be seen, many of these geometries allowed to utterly eradicate the swirl problem, accomplishing also significant pressure drop improvements.

Although the swirl appearance and its consecutive impact, is a primordial factor in a Diesel engine model, the swirl phenomenon and its reduction can be applied to a large number of industrial areas, making the approaches designed in the thesis pertinent from different points of view.

Last but not least, this project will allow the author of the thesis to acquire important CFD knowledge and skills, as well as a valuable labor experience, in this one of the most paradigmatic tools in the fluid and mechanical engineering in the current technological world.

Key words: CFD, Star CCM+, CAD design, Swirl reduction, Pressure drop, Stator, Flow control, Fluid mechanics

Contents

List of Figures

Chapter 1

1 Introduction

1.1 Objectives

The objective of the work hereof is to study several approaches aimed at the reduction of the swirl movement in a pipe through modification of the internal geometry and to analyze their advantages and disadvantages via Computational Fluid Dynamics (CFD) simulations.

Swirl movement can be defined as the helicoidal rotation of the air around the axis of a cylinder. This type of vortex appears in large number of phenomena, among which, the most characteristic industrial example is the combustion chamber of a Diesel engine. This vortex appearance in the Diesel engines is something ineluctable due to the admission geometry, i.e. since the injected air has a certain angular moment, a vortex is induced, and evolves concentrically to the cylinder.

The figure 1 illustrates swirl's structure through a cylinder, that holds a certain similitude to the simplified geometry of a reciprocating Diesel engine, although it can be used for a lot of generic cases based upon swirl propagation. The model, represented via CFD software, is precisely the configuration that, as it will be seen later, was assumed as the starting geometry of this work.
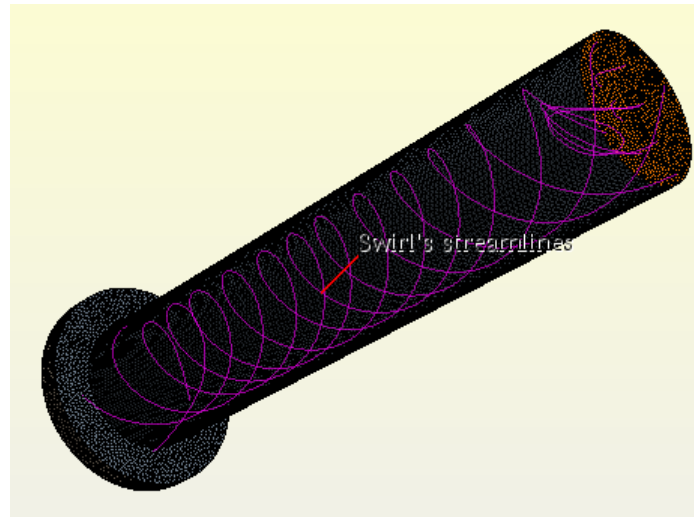
Figure 1: Swirl's formation in the initial project's geometry

As a matter of fact, in many aspects, swirl movement in Diesel engines is something advantageous for the process, e.g. it's propitious for the fuel distribution in the combustion chamber, it's beneficial for the mixture of air-fuel, thus allowing to use much more efficiently the oxygen, and, also, it mitigates considerably the wall-effect. Evidently, a better use of fuel leaves less remaining fuel at the end of the combustion, hence reduces the pollution. However, when the swirl becomes too intense, it may seriously hinder the combustion process.

15

In general terms, swirl leads to pressure losses through the duct, since it creates recirculation zones, as well as it generates aeroacoustic noise. From the aeroacoustic point of view, fluid velocity and the turbulence are the main contribution of the generated noise, which becomes crucial in the phenomenon of swirl, as it is a clear example of a turbulent flow.

Despite the different advantages of the existence of swirl in a duct, the present work is focused on several ways that can be applied in order to modify the internal geometry of the cylinder with the purpose of reducing the swirl as much as possible. Apart from the swirl reduction, another, supplementary, objective of all the designs is to minimize the pressure losses between the inlet and the outlet of the cylinder.

1.2 Previous work

Prior to the beginning of this project, a designed was delivered, result of previous investigations. It consisted on a stator geometry introduced inside of the cylinder, right at its inlet. The exact location and form of the stator can be seen on the figures 35 and 36, both from the upper and side points of view.
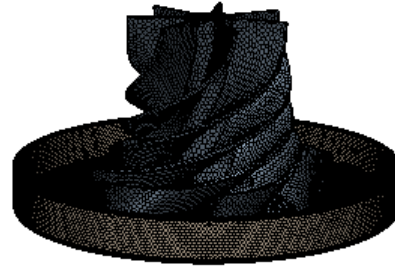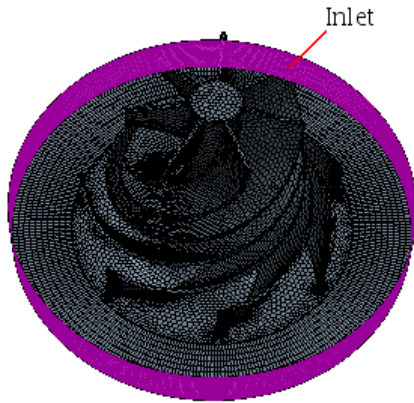
Figure 2: The initial stator (upper view)   Figure 3: The initial stator (side view)

The air is injected into the inlet cylinder, whose walls are marked on the figure 2, in two opposite directions, both perpendicular to the axis of the cylinder. The two injection points are located at the opposite sides of the inlet. Immediately upon forming the swirl movement, the air enters the stator body and is redirected by it, in a way that at the exit of the stator, the flow becomes much more laminar and the streamlines are more parallel among one another. In other words, the swirl structure becomes less conspicuous. Nevertheless, the actual effect of this stator design is very exiguous and does not provide a satisfactory solution to the swirl problem. The figure 4 illustrates the overall geometry of the body with the stator implemented in it and the inlet of the body clearly marked.

The exact values and mechanisms of the problem will be presented in the later part of this thesis. As for now, suffice to say that the tangential velocity at the outlet of the main cylinder at the reference circumference is reduced from 113,47 to 87,52 m/s thanks to this stator model, and the total pressure losses between the inlet and the outlet of the main body are reduced from 23.084 to 20.186 Pa. These results may constitute a sufficient solution for several industrial applications, however, throughout

the development of this document many much more effective designs shall be explained. Some of them are based upon this initial stator design, whereas others are completely independent from it.
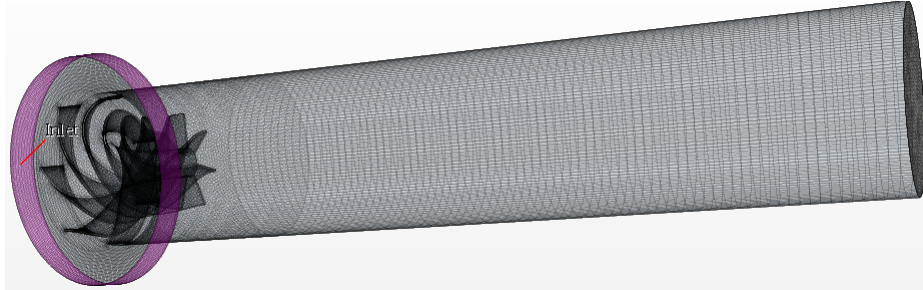
Figure 4: The full view of the initial stator geometry

1.3 Methodology

As has been stated in the chapter 1.1, the different approaches were carried out by modifying the internal geometry inside the main cylinder of the body, that is to say, by adding certain internal bodies whose objective was to alter the propagation of air and to eradicate the helicoidal motion. All the time, it had to be kept in mind that the swirl eradication shouldn't be paid with an additional pressure drop, that usually occurs when the air meets a body on its path and forms recirculation zones, that decrease the pressure. In order to predict the overall effect of each geometry, two basic methods of study are the experimental one, that is to say, an engine test stand, and the computational one, via CFD specialized software.

It is necessary to clarify that in this sort of technological problems, an analytical approach is not feasible, because of an enormous complexity of fluid mechanics phenomena. The paradigmatic set of formulas in fluid mechanics are the Navier-Stokes equations, i.e. a set of partial differential equations based on the conservation equations, that describe the movement of all sorts of Newtonian fluids. However, nowadays there is no analytical solution to these equations, besides certain very simple and determined cases. As a matter of fact, the only viable method of solving the N-S equations is precisely the Computational Fluid Dynamics, CFD.

Regarding the method of an engine test stand, it consists of a technological device that is supposed to be tested, for example the body from this project, and a system that puts the air in motion. The figure 5 shows an engine test stand created by the Detroit subsidiary of the Siemens Corporation, that consists of a diesel engine coupled to an external dynamometer that applies a load equivalent to pulling a 20-ton tow.

Although the figure 5 shows a test stand for analyzing a Diesel engine, the mechanics could be applied to a simple-duct study of a swirl flow inside the body and to determining the relevant parameters. A test stand must include physical parameters sensors or transducers, a data acquisition system and an actuator, in the case presented in the figure 5, a dynamometer. This way a great number of parameters can be determined and evaluated, such as angular moment and velocity, total and static pressures, mass flow, etc. A more sophisticated experimental approach may include Laser Doppler Anemometry (LDA) or Phase Doppler Anemometry (PDA) methods, among many others.

Figure 5: An example of an engine test stand used to analyze Diesel engine's parameters

Nonetheless, the method chosen in this project is the CFD approach. This computational method, developed in the midst of the 60's, consists in solving numerically the Navier-Stokes equations via different possible algorithms and in providing a precise and meticulous analysis of fluid behavior, based on assumed hypothesis and premises. It is considerable less expensive than experimental testing and it has shown a great credibility in an immense number of studies of fluid mechanics. Two most extended CFD software programs in the world are Ansys Fluent and Star CCM+, the latter of which was used throughout the development of this project.

Before proceeding to resolving the problem through the CFD method, an extensive preparatory study was conducted, consisting in performing a set of almost 1.000 pages of official CFD tutorials, of the CD-Adapco/Siemens corporation, covering all the basic aspects of geometry, meshing, flow and automation studying.

In the next chapter, a detailed description of CFD functioning with the emphasis on this project will be explained.

Chapter 2

2 Computational fluid dynamics method: simulation's procedure

2.1 Limitation of the CFD analysis

In the first place, a quick description of the method's limitations shall be presented. Computational fluid dynamics made possible to resolve problems inaccessible ever before with a relatively reasonable cost. However, it is not free of imperfections. One obvious limitation is that for complex problems, it frequently becomes very tedious and onerous to compute all the simulations and in many cases, the full computation requires enormous amounts of hours or, as an alternative, use of very powerful computers.

Regarding the errors inherent to the software code, these can be divided in two parts:

1. Numerical errors: when performing a CFD simulation, it is almost indispensable to compare the results with empirical data, or, at the very least, with results of other simulations, previously corroborated through different methods. That is so, since the numerical code itself is usually very complex and correcting it is utterly impractical. Additionally, the physical models assumed are usually very different to evaluate. With respect to the algorithms used to solve the N-S equations, each algorithm has its own method of measuring and correcting the numerical error and the algorithms vary enormously from one to another, thus making it impossible to apply a generic procedure of code correction.

2. Numerical diffusion: with this term several convergence errors are described, among which there are:

- Cells with a high aspect ratio (skewness)

- Linearization of the equations

- Truncating of numbers methods

This way, it is possible that the residuals of the simulations, which represent in simple terms the differences between the previous and the current iteration, are very small, but the case has not reached convergence in spite of that. Convergence can be improved by several paths, such as refining the mesh, using double precision methods, lowering the under-relaxation factors, or simply changing the physical model.

In designs that attempt to choose the optimum solution to a particular problem, such as the design carried out in this project, usually by definition there are no experimental data that can be compared to the simulations' results. Nevertheless, that doesn't refuse the idea that the computational study may provide very coherent and useful information about the best industrial solutions, both from the qualitative and quantitative points of view.

In any case, being able to estimate and predict these imprecisions and errors may be enough in order to present reliable results, bearing in mind that they will only represent a good approximation of the reality.

2.2 Detailed description of the process

In this paragraph, all the steps involved in a CFD analysis will be presented and explained. The real model from the project will be used in order to illustrate all the pertinent concepts. CFD processes follow an established chain of stages, that can be classified into three groups: preprocess, solver and postprocess.

2.2.1 Preprocess

This stage covers all the steps prior to the actual simulation and computing of the conservation equations. The steps are the following ones:

- Creating or importing the relevant geometry

- Generating the appropriate meshing of the geometry

- Establishing the physical and chemical models of the process

- Defining material properties

- Defining a complete set of boundary conditions

In this stage, all the relevant activities must be carried out in a sedulous and adequate way, because all the results of the simulation will be determined by the hypothesis and premises assumed in the preprocess. A particular difficulty resides in a correct meshing refinement, that must be adjusted and customized according to the requisites and characteristics of every geometry. Mesh refinement is thereby an individual process that cannot be applied via generic set of rules.

In the following pages, a detailed description of all these steps will be given.

2.2.2 Preprocess: geometry

Star CCM+ presents a great variety of tools for designing all kinds of geometries, as well as allows the user to import any design from external programs, e.g. Catia, Unigraphics, NX, etc. In this project, most of the designs were constructed from the beginning, except for those based upon the initial stator design.

Regarding the basic constructed geometry, the initial idea is just based on two joint cylinders, such as can be seen on the figure 6. The base cylinder has a larger diameter than the main cylinder and the exact parameters of the geometry can be read on the figure 7. Regarding the design, the first thing was to create a *sketch* in form of a circumference and to use the command *extrude*, in order to create a solid body. Afterwards, another sketch was created on the surface of the base cylinder, a sketch which is marked in green on the figure 6. Analogically, a second extrusion was performed in order to create the main cylinder, which is marked in yellow on the figure 6. It is important to emphasize, that the geometry does not represent necessarily any part of a Diesel engine, and all the procedures used in the project hereof can be applied to different kinds of industrial products.

This is the starting point for all the future designs presented in this project. Starr

CCM+ offers a variety of tools that allow to create even the most complex geometries. Once the CAD design is completed, the next step is to create a new *part* from it. This is the option that informs the software that the designing of the geometry is finished and the user will be able to manipulate the different components of it manually, using the different available commands. Some of the basic commands to manipulate a part are: *combine, transform* and all sorts of *boolean* operations, as well as *splitting the geometry* into different elementary components and to be able to name them appropriately. Consequently, the user has to assign the finished part to a *region*, which will complete the creation of geometry in Star CCM+.
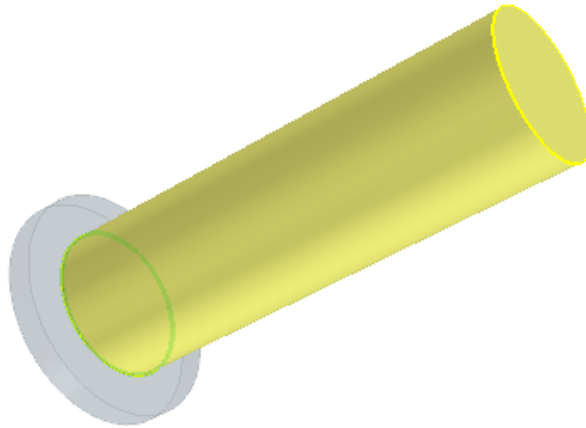
Figure 6: The initial created geometry

Parameter	Value (m)
Base cylinder's diameter	0,205
Base cylinder's height	0,023
Main cylinder's diameter	0,135
Main cylinder's height	0,650

Figure 7: The values of the initial geometry parameters

It is important to state that all the basic steps of Star CCM+ have their respective forms in other CFD software, such as Ansys Fluent and Converge. Although the exact commands and the interface vary, the conceptual ideas have no changes whatsoever.

As it has been stated so far, all the new designs in this project were just modification of this basic geometry, except for the original stator design, from previous projects, that can be seen on the figure 2. This stator had been created in a separate CAD program, since the complexity of its design would make it too tedious to create in a CFD program, although it would also have been perfectly viable.

21

2.2.3 Preprocess: meshing

The next step of any CFD process is to create the meshing of the geometry, that is to say, to divide the geometry into finite volumes that will enable the solver to perform the necessary iterations and to compute the values of all the desired physical parameters. This step is primordial in a preprocess stage, since the quality of the outcome will be based upon the quality of the mesh.

In Star CCM+ the procedure that was followed, consisted in create a new *operation* called *automated mesh*. After assigning this operation to the existing part, three *meshing models* were selected. The first one was a *surface remesher*. This consists in creating a number of cells, i.e. finite volumes, on the faces of the body. Two additional adjustments selected for this meshing model were *curvature refinement* and *proximity refinement*, that refined the meshing in the curves and in the proximities of geometric singularities, in order to create a much more veracious representation. The figure 8 shows the outcome of the model for the initial geometry of the problem.
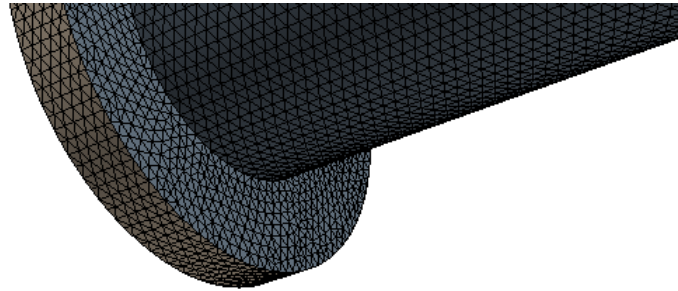
Figure 8: The initial mesh in form of tetrahedra

The second meshing model is the polyhedral mesher, which divides the entire volume of the body into finite volume cells, in forms of tetrahedra, which are then converted to polyhedral-shaped cells. An alternative would be to leave the cells in forms of tetrahedra, however there are studies that show the advantages of using the polyhedral-shaped cells instead of tetrahedra, as explained in the reference [9]. The figure 9 shows the volume mesh created that can be contrasted to the surface remeshing shown on the figure 8.
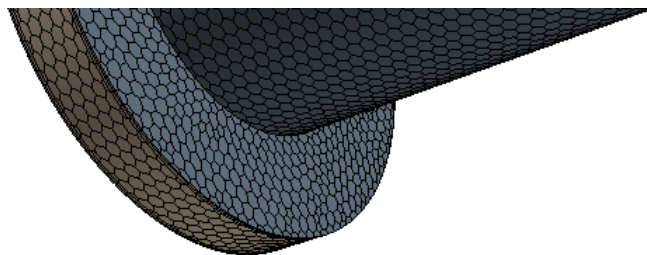
Figure 9: The polyhedral improved mesh

The third model is called prism layer mesher and it deals with all the aspects of boundary layers in assumption of a viscous fluid. The flow may become complex near the walls of the geometry, and, in particular, it is theoretically null immediately next to the wall. The *law of the wall* in fluid mechanics states that the average velocity of a turbulent flow at a certain point is proportional to the logarithm of the distance from that point

to the "wall", or the boundary of the fluid region. Since in this project the flow is both viscous and turbulent, the phenomena pertaining to the wall's proximity must be taken into consideration. In Star CCM+, in order to capture these phenomena accurately, several layers of prismatic cells are created via this third meshing model. On the figure 10, a close look at two prism layers at the outlet of the body, that is to say, in the upper face of the main cylinder, is shown.
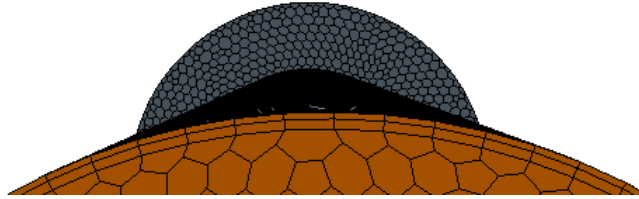
Figure 10: A detailed look at the prism layer meshing

After selecting all the pertinent meshing models for the basic geometry of the project, certain numerical value of meshing parameters must be introduced. The most important one is the *base size* of the cell. It is not possible to foresee the value of this parameters a priori, thereby a parametric study must be carried out, called *mesh independence study*. The exact process of this study will be shown in the explanation of the main proposed solution. As for now, suffice to say that the parameters of the mesh for the basic geometry were established, and that for this first geometry, there was no need for *customizing the mesh*, i.e. for refining it in certain particular places, due to the simplicity of this first design. The figure 11 illustrates the most relevant parameters for the basic geometry mesh.

Meshing parameter	Value (% of the base size)	Absolute value
Base size	100	0,005 m
Target surface size	100	0,005 m
Minimum surface size	10	0,0005 m
Number of prism layers	-	2
Prism layer thickness	33,33	0,00167 m
Total cells number	-	93.146 (-)

Figure 11: Meshing parameters for the initial constructed geometry

As it has been stated earlier, the stator geometry, imported from the previous projects, does not follow the exact same procedure. The meshing parameters are slightly different to those described on the figure 11 for the basic geometry. Nonetheless, the main difference is that the mesh was not created via an automated mesh operation, but by creating a new *mesh continuum* in the *continua* tree. A fourth meshing model was also selected, which in this case was an *extrusion meshing*. In other words, this means that only a part of the full geometry was created in the geometry step, and only this part was meshed, following the first three models explained so far. The rest of the geometry was created and meshed in the meshing process, through prismatic cells, in order to simplify the meshing in those places, that weren't really that complex for the flow simulation and it was more beneficial to reduce the computational cost with this procedure. The figure

12 illustrates the so obtained mesh. The extrusion was applied in two places. Firstly, only part of the base cylinder was constructed; the full diameter was not created in the CAD design, but was later added in the extrusion meshing process, as can be clearly observed on the figure 12. Secondly, only a part of the main cylinder was extruded in the geometry design, the rest was extruded in the meshing process, as can be also observed on the figure 12.
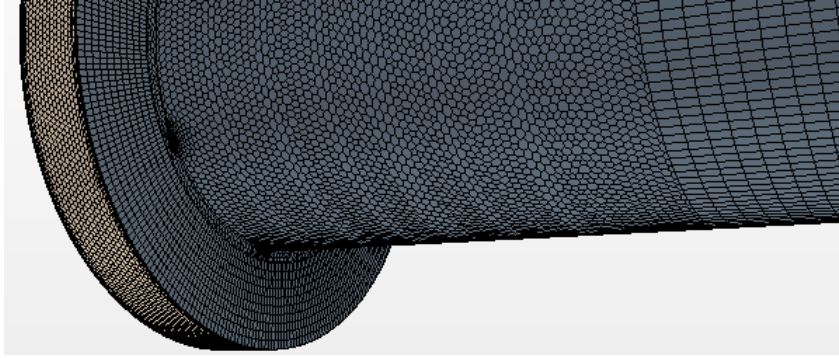
Figure 12: The mesh obtained via the extrusion meshing option

2.2.4 Preprocess: physical models and material properties

In the next step, a set of physical models was selected, in order to create a high similitude between the simulation and the real-world processes. Evidently it becomes utterly impossible to reflect all the phenomena present in the real world, since the computational possibilities of CFD have yet to be perfected. Hence, a set of simplified yet coherent approaches must be chosen.

Spatial model

The model chosen in this aspect was a full *three-dimensional* representation, with no symmetry assumptions whatever. That is so because the designs created in the project very often don't follow any particular symmetry and the flow inside the cylinders is generally also asymmetrical.

Temporal model

The model chosen is a *steady flow*, since the boundary conditions for the problem are constant and the inlet mass flow doesn't vary, as it will be seen in the next step description. A brief description of a transient approach will be presented in the next parts of the document.

Flow and fluid models

Concerning the flow type, the model chosen for the fluid description is the *constant density* one. The fluid used throughout the project is the air only, and it will not reach high velocity, $M > 0,3$ in any moment. Apart from it, aspects of temperature, chemical reactions or abrupt and large pressure changes will not be present in this project's problem, thereby a constant density assumption is congruent. The value of the density was chosen as $0,85 kg/m^3$ and the dynamic viscosity as $1,85 \times 10^{-5} Pa \times s$.

Regarding the flow itself, the way of computing it is via a *segregated flow*. That is to say, the conservation equations are computed independently from one another in each iteration. An opposite approach would be a *coupled flow*, in which the conservation equations are solved altogether. By using the segregated flow, the computational cost is reduced, since the computer does not have to memorize the equations at each step, and the RAM memory is not consumed in such a significant way as in the coupled model. Nevertheless, this model makes the convergence more difficult to accomplish, thus making the convergence reaching considerably slower.

Turbulence models

The vast majority of problems present in fluid mechanics are turbulent, i.e. have the Reynolds number higher than a certain value, that varies for the geometry for the problem. Turbulence is a highly complex phenomenon that presents characteristics such as three-dimensionality, diffusivity and little predictability. The flow in the problem of this project forms a swirl, which is a typical example of a non-laminar flow, with a great angular momentum and vorticity. Its turbulence scale is so high that it's comparable with the characteristic geometry of the problem.

There exist three basic approaches for the turbulence computation:

- *Direct Numerical Simulation (DNS)*: this model computes all the turbulence scales numerically. The mesh refinement has to be so small that it covers even the smallest Kolmogorov turbulence scales. The time step for the transient simulations must also be small enough to cover the periods of the fastest turbulent fluctuations. An immediate and inexorable consequence is that this method has tremendous computational costs, thereby it has almost no industrial applications whatever, except for simple geometries involving incompressible flows.

- *Large Eddy Simulation (LES)*: in this method, the larger turbulence scales are computed directly, whereas the smaller ones are modeled. The mesh size acts as a filter that doesn't cover the smallest vortexes. The computational cost is smaller than in the DNS method. It is still however little practical nowadays.

- *Reynolds Averaged Navier-Stokes equations (RANS)*: this is by far the least expensive and the fastest of the three methods. The main point is to decompose all the pertinent variables in their average and fluctuating components via a so called *Reynolds decomposition*. The equation 1 illustrates a trivial example for the velocity parameter.

$$u(t) = U + u'(t) \tag{1}$$

This is precisely the method chosen for describing the turbulence in all the designs of this project. An example of N-S equations for a stationary, incompressible and Newtonian fluid is shown through the complex equation represented on the figure 13.

$$\rho \bar{u}_j \frac{\partial \bar{u}_i}{\partial x_j} = \rho \bar{f}_i + \frac{\partial}{\partial x_j} \left[-\bar{p}\delta_{ij} + \mu \left(\frac{\partial \bar{u}_i}{\partial x_j} + \frac{\partial \bar{u}_j}{\partial x_i} \right) - \rho \overline{u_i' u_j'} \right]$$

Figure 13: N-S equation for a stationary, incompressible and Newtonian fluid

After decomposing the magnitudes through the Reynolds decomposition and simplifying the expression, one can arrive at the equation shown on the figure 14.

$$\rho \bar{u}_j \frac{\partial \bar{u}_i}{\partial x_j} = \rho \bar{f}_i + \frac{\partial}{\partial x_j} \left[-\bar{p}\delta_{ij} + 2\mu \bar{S}_{ij} - \rho \overline{u'_i u'_j} \right]$$

Figure 14: A simplified version of the previous N-S equation via a Reynolds decomposition process

Due to the empirical nature of the RANS method, there is no generic way of describing turbulence through this model. There is a great number of different approaches that must be selected accordingly to the problem of interest. In this thesis, the RANS model selected is *k-omega*. In this model, there are two turbulence partial differential equations, for two variables. The first one, k, represents the *kinetic turbulence energy*, whereas the second variable, omega, represents the *turbulent dissipation*, i.e. the ratio of transformation of the turbulent kinetic energy into thermal energy.

An additional and the last model for the turbulence used in the project is the *Shear Stress Transport model (SST)*, developed by F.R. Menter in 1993. This model uses two eddy-viscosity equations, combining the best approaches from k-omega, and k-epsilon models, as explained in detail on the website referenced by [14]. This way, the SST k-omega approach computes in a meticulous way the flow behavior near the boundary layer, as well as presents reliable solutions for the free-stream flow.

All these physical models were the same both for the designs based on the constructed geometry as well as for those based upon the imported stator design.

2.2.5   Preprocess: initial and boundary conditions

The initial conditions are very influential upon the stability and convergence of the solution, even considering that they will not influence the final solution, since the case studied is stationary. The table shown on the figure 15 describes all the relevant initial conditions of the problem.

Parameter	Value
Reference pressure	101.325 Pa (atmospheric)
Working pressure profile	0,0 Pa
Turbulence intensity	0,01 (1%)
Turbulence velocity scale	1 m/s
Turbulence viscosity ratio	10

Figure 15: The summary of the problem's initial conditions

With respect to the boundary conditions imposed to the geometry, these are constant throughout all the designs created in this thesis. All the elements of the basic geometry, as well as all the elements of other geometries, are always standard, wall boundary conditions. The inlet of all the geometries is the lateral wall of the base cylinder and its boundary condition is assigned as a *mass flow inlet*. The mass flow entering the

26

inlet is constant and its value is imposed as $0,7kg/s$. In order to establish its direction, a cylindrical system of reference had been created. The radial axis direction of the reference system is [1, 0, 0], the tangential one is [0, 1, 0] and the axial one is [0, 0, 1]. According to this system, the inlet flow direction is [-0,577; 1,0; 0,0]. The exact configuration is illustrated on the figure 16.
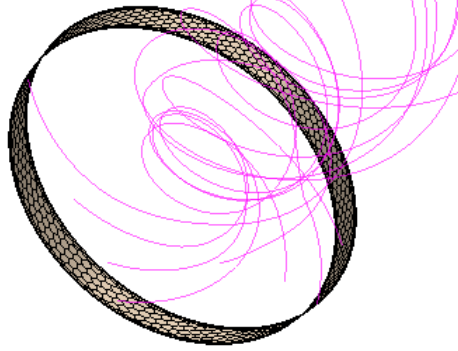
Figure 16: The initially-formed swirl due to the problem's boundary conditions

Finally, the outlet of all the designs, i.e. the upper face of the main cylinder, was established as a *pressure outlet* boundary condition.

2.2.6   Solver: mathematical description

In this paragraph, a detailed overall look shall be presented, pertaining to the solver used by all the simulations of this project. In the first place, as it was stated previously, the solver used was a *segregated flow* solver. Its characteristics are that it computes the continuity and the momentum equations independently one from another, because of which, the computational costs are lower, although the convergence may become slower, than in the *coupled flow* solver. The linkage between the momentum and continuity equations is achieved with a predictor-corrector approach.

In the second place, it is important to stress that there are different segregated flow solvers, such as SIMPLE or SIMPLEC algorithms, however, in this chapter, a generic procedure of this solver will be depicted. Another pertinent concept is that this model has its roots in constant-density flows. Although it is capable of handling mildly-compressible flows and low-Raleigh-number natural convection, it is not suitable for shock-capturing, high Mach number and high Raleigh-number applications. Thereby, for this project's purposes, this solver is very adequate, due to the constant density assumption, as it was stated previously. The figure 17 illustrates the basic scheme of this solver, whose steps are the following ones:

1. For each iteration, the physical parameters (thermal conductivity, viscosity, etc.) are calculated from the previous iteration's outcome. For the first iteration, the solver simply takes the initial conditions values

2. The velocities in all three directions are solved through the momentum conservation equations, using the current values for pressure and face mass fluxes.

3. The next step is to solve numerically the continuity equations, however the velocities obtained in the step 2 may not be congruent. For that reason, a Poisson-type equation for

the pressure correction is derived from the continuity equation, in order to calculate the necessary corrections for pressure, velocities and mass fluxes. This way, the continuity equation is satisfied.
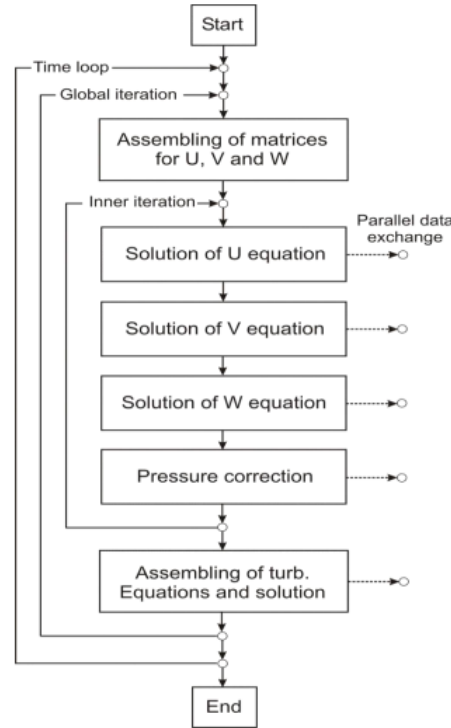
Figure 17: The generic scheme for the segregated flow solver

4. Finally, equations for scalars such as turbulence and energy are solved using the updated values of the other variables.

These steps are repeated for as many iterations as needed, until reaching convergence of the case. A more detailed insight on the convergence analysis will be presented in the next paragraph.

2.2.7 Solver: tools for determining the convergence

The main instrument to use while evaluating the convergence in CFD is the study of *residuals*. These can be defined as the local imbalance of a conserved variable in each control volume. In other words, they give an approximate idea regarding how small the difference is between the last iteration and the current one. Residuals will be different for each cell of the mesh and for each of the solved equations. Each CFD code will have its own procedure for normalizing the solution residuals. In any numerical method, they will never reach exactly zero, nevertheless, the smaller they are, the bigger the probability that the simulation has reached its convergence.

The figure 18 illustrates the residuals plot for the basic project's design, composed of only base and main cylinders in its geometry. Starting from approximately 800th iteration, the residuals reached very low and constant values for all the studied conservation

equations, making it very probable that the convergence was reached.
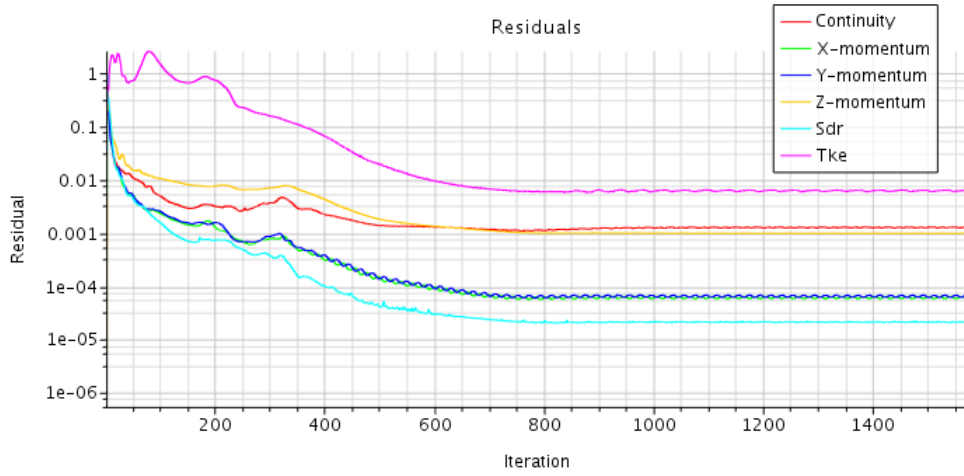
Figure 18: Residuals plot for the initial geometry

The second method of evaluating the convergence of a simulation, that is to say, evaluating whether or not the current results can be assumed as definitive, is to study some selected parameters and observe their evolution with the progress of each iterations. To this purpose, a *report* must be created, in other words, a tool providing the current numerical value of a chosen parameter in a chosen part of the geometry. A report can be run if the simulation is stopped, and the correspondent value can be read in the output window, however, a much more convenient method is to *create a plot* from the report. In this way, the selected magnitude can be visualized with the progress of the iterations, the same way as it is done in the case of residuals.

In the designs of this project, several plots were created for each design. However, in order to clarify the method, one plot will be presented, that has been used for the development of all the designs, that is to say, the static pressure drop. This report measures the difference in the static pressure for two assigned parts, which in these geometries have always been the inlet and the outlet. As it was stated before, the pressure difference is one of the main aspects that must be taken into consideration when designing swirl reduction geometries.
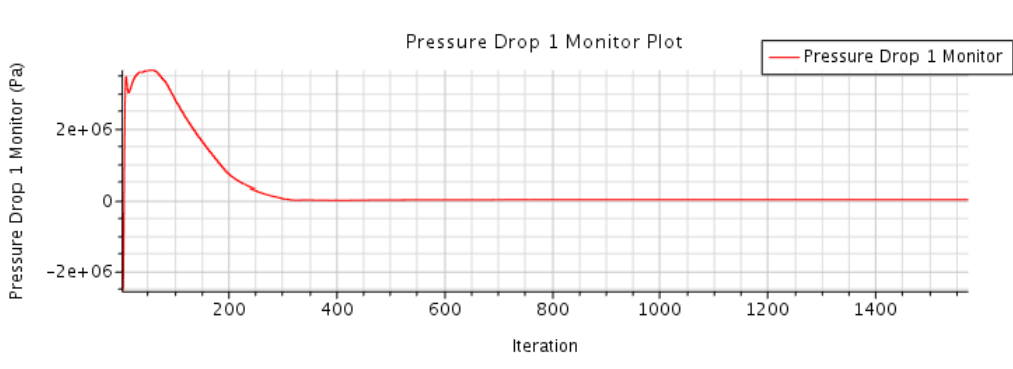
Figure 19: The plot for the static pressure drop

The figure 19 shows the evolution of the static pressure difference along the iterations, for the basic geometry of the project.

The figure 20 shows the final interval of the simulation in detail, in order to illustrate the behaviour of the variable after a certain number of iterations. It can be seen, that the convergence is not perfect, since there are still slight variations of this parameter. Notwithstanding, the maximum variations is of the order of $1 \times 10^2 Pa$; taking into account that the value of the static pressure drop for instance in the iteration 1.570 is about 18.950 Pa, this variation represents about 0,5 per cent of the total number, making it little conspicuous.
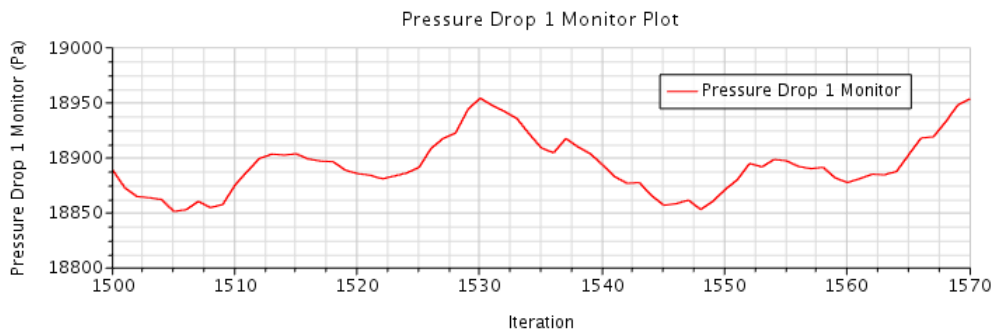
Figure 20: The plot for the static pressure drop in detail for the final iterations

In spite of being able of accepting the values given by this simulation, there are some CFD tools that allow to improve the convergence. The main one is the *under-relaxation factors* study (URF). The URF's are the coefficients that need to be multiply by the solution for each variable, and they span from 0 to 1. In Star CCM+, in the *Solvers* block, it's possible to choose the URF's and to establish their values. In this project, there were always two URF's, one for velocity and the other one for pressure. The fastest option is when a URF has the value of 1, however, convergence problems may appear. In order to improve the convergence, a good approach usually is to reduce the under-relaxation factors and to observe the difference. In some designs, as it will be seen later, this method will be taken into account.

Another way, somewhat riskier, is to change the physical model of the solver. An example in this project would be to change the model for the air from constant density to *ideal gas model*. This way, the gas will be incompressible and it will follow the ideal gas law. Nevertheless, it might not be very coherent to simulate some designs with one physical model and others with a different one. The so obtained results may not be very credible and veracious.

As a final mention for the solver description, it is relevant to emphasize, that Star CCM+ has also the option of applying *stopping criteria*, that is to say, finishing the simulation in an arbitrary way estimated prior to running a case. This can be accomplished either by an arbitrary number of iterations or by an *abort file*. Since it is not a precise and credible way of evaluating convergence in this kind of problem, throughout the development of this project, this option was not used in any of the designs studied. The convergence has always been determined via residuals and parameters study for several variables.

2.2.8 Postprocess: plots and derived parts tools

After finishing running a simulation, the next stage is to obtain all the results of interest for the case. Obtaining as much apposite information as possible from the simulation will constitute the postprocess of CFD. One way is to run the created reports or to observe the plots for each variable, created from the reports prior to the simulation process.

In all the designs of this project, four reports with their respective plots were created. In the first place, the static pressure drop report, between the inlet and the outlet of the geometries, was created. In the second place, a report showing the total pressure at the inlet of the geometry was created for each design. The same was done for the total pressure at the outlet of the body. With these to total pressure reports the objective was to subtract the value at the outlet from the value at the inlet, since there is no specific total pressure drop report in Star CCM+.

The fourth report measured the swirl magnitude at the outlet of the body. Star CCM+ allows the users to create the so called *derived parts*, i.e. geometric elements that are used exclusively for the postprocess purposes, and do not influence directly the results. A cylindrical derived part was created in the proximity of the outlet, in such way that it intersected perpendicularly the outlet forming a circumference of radius of 0,057 m. For this circumference, a *surface average report* was created, that is to say, a report that shows the average value of a parameter onto a specific surface or line. The parameter selected for the surface average was the tangential velocity. By doing this, it was possible to determine the tangential velocity of the flow at the external part of the outlet, which helped estimate the swirl's intensity and the influence of a particular design on swirl reduction. As it has been said so far, all the four reports were created for all the designs.

2.2.9 Postprocess: scalar scene analysis

Star CCM+ allows to create different sorts of scenes in which the user can visualize numerous parameters. Two examples are a *geometry scene* and a *mesh scene*, that have been used in order to visualize all kinds of geometry and the meshing details. However, the type of scene mostly used for determining the results in this project was the *scalar scene*. This scene allows to illustrate a great number of scalar parameters over specific surfaces, either those belonging to the geometry or to a derived part created manually. Of course, this can also be applied for vector parameters via a *vector scene*, not required however in this project.

On the figure 21, the scalar scene for the basic geometry, without a stator, is shown, illustrating two planes, one derived plane axially positioned along the longitudinal axis of the main cylinder, and the other one is the outlet plane, containing the derived section in form of circumference, described earlier. The scalar parameter shown in the figure is the total pressure distribution along these two planes.

Thanks to the scalar scenes, the user can grasp the whole parameter's distribution in the parts of interests and evaluate the necessary concepts in order to improve the outcome accordingly to the specific problem. Another additional derived part created in this project's designs are the flow's *streamlines*. In this case the streamlines' parameter is the velocity. These lines illustrate, in summary, the positions and the directions of the flow along the whole geometry, from the inlet until reaching the outlet. The figure 21

also includes the representation of the streamlines for the basic geometry of the project.
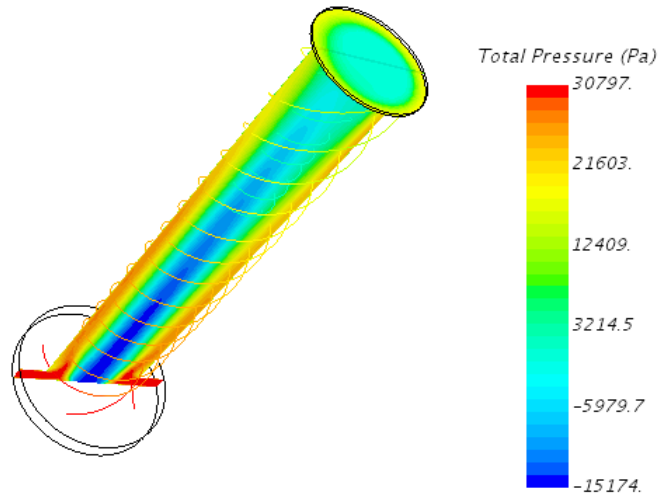
Figure 21: The scalar scene for the total pressure along with the flow's streamlines for the initial geometry

Chapter 3

3 Exact description of the project's problem

In this chapter the explanation of both initial geometries, along with their numerical simulations' results, will be presented. In the first place, the basic design without the stator will be described. Afterwards, the same shall be done for the design based upon previous work, i.e. the geometry with an included stator construction.

3.1 Main project's geometry

As it has already stated, the main geometry for this project is composed of two joint cylinders, one that is used as the base and contains the inlet, and the second one used as a duct, which ends in the body's outlet. The figure 1 illustrated it, as it was stated before. This geometry was imposed initially as something inalterable, thereby all the designs hereafter must abide by its constraints. It was built by the author of this thesis at the very beginning of the project, according to the data provided for it.

All the CFD phases for the base geometry have already been described in the chapter 2. These phases will be very similar for all the designs that do not include a stator. Figures 19 and 20 represent the static pressure drop plot, generally and in detail, respectively. As stated in the chapter 2, four reports had been created for this simulation. As seen in the figure 20, static pressure drop for the basic problem has the value of 18.918 Pa, according to the report, that is to say, approximately 19 bar. This value will have to be compared to all the analogical reports in the designs henceforward.

The figure 22 illustrates the plot for the total pressure inlet and the figure 23 shows the plot for the total pressure outlet.
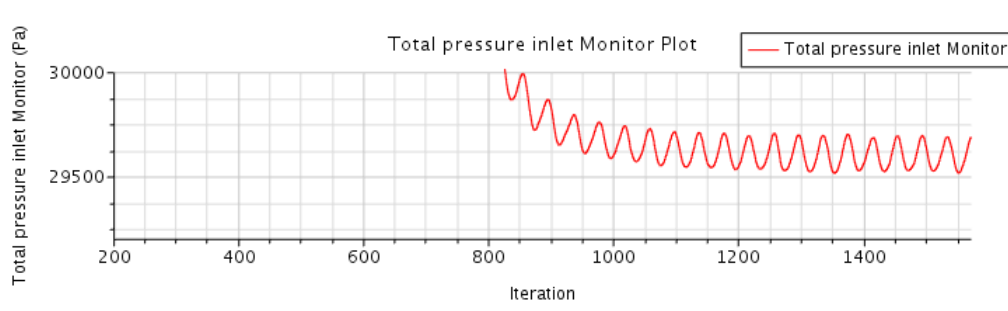
Figure 22: The plot for the total pressure parameter at the inlet

The same way as in the figure 20, it can be observed that the convergence is not perfect. This can be noticed especially in the figure 22, due to the purposely adjusted y-axis. Notwithstanding, the same way as in the figure 20, the present variations are inconspicuous in comparison to the value of the parameters at the corresponding iterations, thus convergence assumption is feasible.

The outcome value in the figure 22 is 29.498 Pa according to the report, and the value in the figure 23 is 6.413 Pa. Hence, the variation of the total pressure between the

inlet and the outlet in the initial geometry is 23.084 Pa. It is fundamental to remember throughout this project that the main objective of it is to reduce the swirl movement as much as possible, eradicating it in the best-case scenario, i.e. reducing the total pressure drop is a secondary objective, supplementary to the swirl reduction in any case. However, it will be attempted to mitigate this drop if possible.
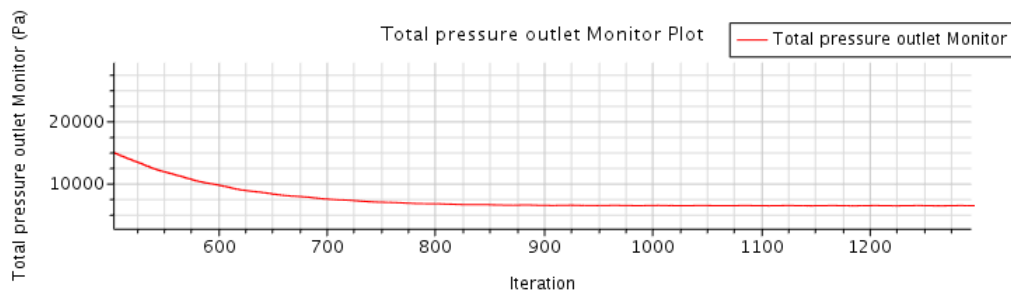
Figure 23: The plot for the total pressure parameter at the outlet

Finally, the figure 24 shows the plot for the tangential velocity averaged along the circumference created as an intersection between the outlet and the cylindrical derived part.
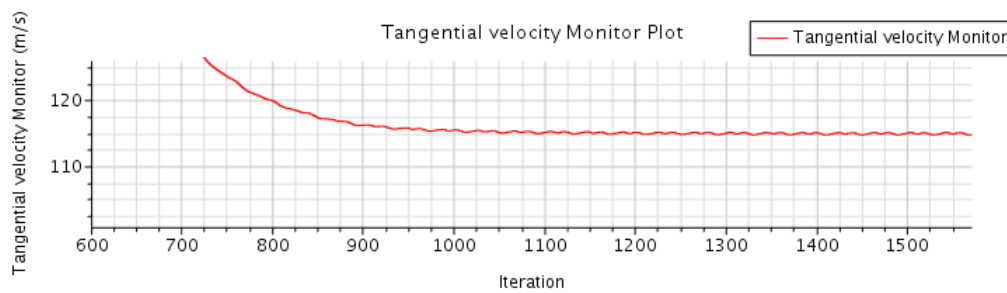
Figure 24: The plot for the tangential velocity at the created derived part

Report analyzed	Value upon reaching convergence
Static pressure drop (Pa)	18.918
Total pressure inlet (Pa)	29.498
Total pressure outlet (Pa)	6.413
Total pressure drop (Pa)	23.084
Tangential velocity (surface averaged) (m/s)	113,47

Figure 25: The summary for the results for the initial geometry of the project

It can be observed that this value upon converging is $113,47 m/s$, according to the report. This is thereby the main reference point in the whole project. The table shown on the figure 25 summarizes the results for the basic geometry of the problem.

Finally, the figure 21, shown in the previous chapter, illustrates the scalar scene with total pressure distribution, as well as with streamlines. It can be seen, that the helicoidal motion is fully developed, presenting an emblematic case of swirl movement. Inside the swirl there is an abrupt decrease in pressure, since the flow follows an axial-tangential trajectory close to the walls of the duct. The designs presented in this project will attempt at altering this trajectory as much as possible.

3.2   Basic geometry based on previous work

As it was stated in the chapter 1.2, the design containing the stator had been created prior to the beginning of the project hereof. The stator's construction was built in an external CAD software and then imported to Star CCM+. The figure 4 shows a general view of this design, while the figures 2 and 3 show the detailed look at the stator part specifically.

The main problem with this approach is that since it was not built from the beginning in Star CCM+, there is no direct way to edit the design parameters in the 3D-CAD model of the CFD program. Evidently, there are different ways to modify this geometry, however, because of it, the most practical and safe option will not be viable.

Another crucial difference with respect to the basic geometry explained in the section 3.1, is that in the basic geometry design, the whole construction is established as a fluid body, whereas in the stator design, it is not. This means that in the basic geometry, the whole body represents the domain in which the fluid can move, and the walls of the body act literally as solid isolation for the fluid. Most modifications in the geometry used CFD functions *extrusion cut* and *revolve cut*, that cut axially or cylindrically through the fluid body, creating this way new solid walls inside the body, that will redirect the flow.

In the stator design however, all the imported features act as solid walls in the stage of designing and modifying the geometry, and the empty space among them is precisely the fluid domain. This characteristic makes the step of modifying the stator geometry much more complex than editing the basic geometry of this project.

The conceptual idea of implementing a stator consists in redirecting the flow entering cylindrically through the whole inlet wall, in a way that it meets the stator's blades right upon its entrance. Due to the curvature of the blades, these redirect the flow and are supposed to transform it into an axial flow, much more laminar than before. The scalar field of the total pressure along with the corresponding streamlines are shown in the figure 26. It can be seen how the stator influences indeed the streamlines, in comparison to the figure 21, and making them much less developed and constant. The pressure gradients are also much less conspicuous than before. Nevertheless, the flow is still highly turbulent and presents a highly intense swirl.

The figure 27 shows a detailed view of the influence of the stator upon the streamlines right at the stator zone. Now it can be clearly observed how the stator does indeed fulfill its conceptual purpose, but only to a certain extent. Only a part of the streamlines is captured by the stator's blades, and even then, the streamlines quickly leave the stator's geometry, escaping laterally. Thus, the stator's theoretical objective is not truly satisfied.

The results of the simulation, after having followed exactly the same scheme as in the section 3.1, show a slight improvement in comparison to the basic geometry. Static

pressure drop is now 16.596 Pa, according to the report, which constitutes a 12,27 per cent improvement in comparison to the basic geometry. The static pressure plot created from the report can be seen in the figure 28. As well as before, the convergence is not perfect either, since the parameter has certain periodic oscillations upon reaching a certain number of iterations; these oscillations however, are just a tiny percentage of the total values, making it reasonable to assume full convergence.
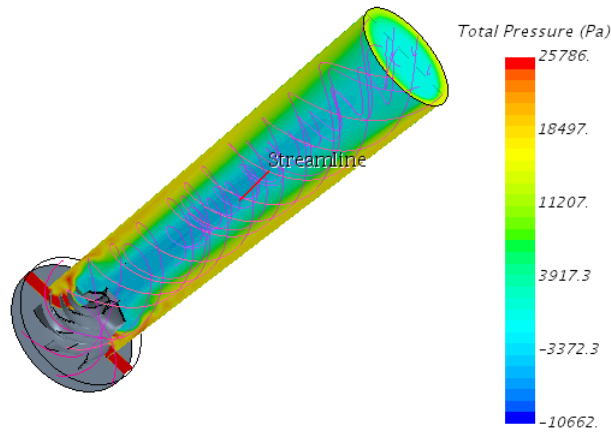
Figure 26: The scalar scene for the initial stator geometry along with the streamlines
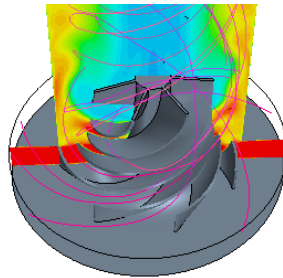
Figure 27: The detailed view at the streamlines in the stator region
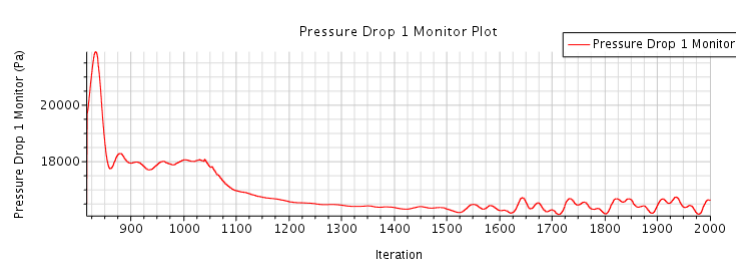
Figure 28: The plot for the static pressure drop

The table shown on the figure 29 gives the results for the three most relevant parameters, as well as their difference with respect to the non-stator geometry. As it can be observed, the stator's blades reduce the swirl, producing a decrease of tangential velocity at the circumference upon the outlet in 22,87 per cent. Apart from it, this swirl reduction does not cause any static nor total pressure difference increase, just the contrary, it reduces

it in 12,27 and 12,55 per cent respectively, as it has already been noticed in the total pressure gradients diagram from the figure 26.

Parameter of interest	Value	Improvement in relation to the non-stator geometry
Δ Static pressure	16.596 (Pa)	12,27%
Δ Total pressure	20.186 (Pa)	12,55%
Tangential velocity (surface averaged)	87,52 (m/s)	22,87%

Figure 29: Summary of the results for the initial stator geometry

The overall conclusion for the stator design prepared in previous work, is that it is indeed somewhat beneficial to the problem's improvement, nevertheless, its performance is far from being satisfactory. As it will be seen in the next chapters, there is a great number of far more favorable and efficient ways of reducing immensely the swirl as well as decreasing the static and total pressure drop.

Chapter 4

4   Proposed main solution

As it has been stated in the chapter 3, there are two initial designs for the project, the first one described in the chapter 3.1, constructed and simulated from the beginning, by the author of this thesis. The second one, described in the chapter 3.2, contains a stator design created prior to the commencement of this work. Both present the same swirl problem; the stator design aimed at reducing the swirl and improving the pressure drop, which was indeed accomplished, as seen in the table of the figure 29, however, only to a certain extent, far from being satisfactory for future industrial projects where the swirl is not desired.

In this chapter, the main concept for swirl reduction, designed by the author of the project, will be meticulously depicted. In total, 19 variations of this concept have been carried out and simulated, including the mesh independence study and several parametric studies, in order to select an optimum model, both from the swirl and from the pressure drop points of view.

4.1   Explanation of the main concept

The main idea hinges upon the concept of breaking the swirl movement by locating a plate (or several plates) parallel to the main cylinder's longitudinal axis. The air flow upon encountering it suffers an abrupt and intense stop, that causes strong turbulence and a drastic change in flow's motion. When it leaves the plate's zone (or the grid formed by several plates located perpendicularly to one another), the flow is no longer influenced by the boundary conditions at the inlet, but the preponderant factor is now the influence of the plate. In summary, the plate disables the swirl to propagate smoothly and inalterably through the main duct.

The first approach consists in one, 2 mm - thin plate situated in an utterly arbitrary point of the duct, as it is illustrated in the figure 30. The meshing has been put transparent in order to enable the visualization of the interior of the body. This design's name is "idea1.0".
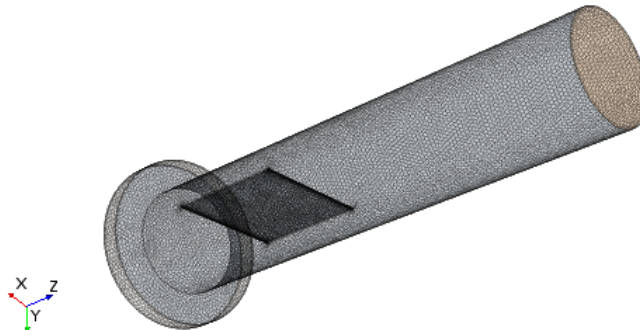
Figure 30: The first proposed solution for the problem

All the designs from this chapter are based entirely upon the basic design described

in the chapter 3.1. Thereby, as it has already been stated, all the plates have been extruded via the *extrude cut* function in Star CCM+, from sketches drawn upon XY and YZ CAD planes. These new geometries were exported to new parts, assigned to regions, and all the steps described sedulously in the chapter 2 were applied, in a very similar way to the one for the initial design.

The outcome of this first approach was far more satisfactory than the basic stator design in the aspect of swirl reduction. Figure 31 shows the scalar scene of the total pressure distribution for this design, as well as the streamlines configuration.
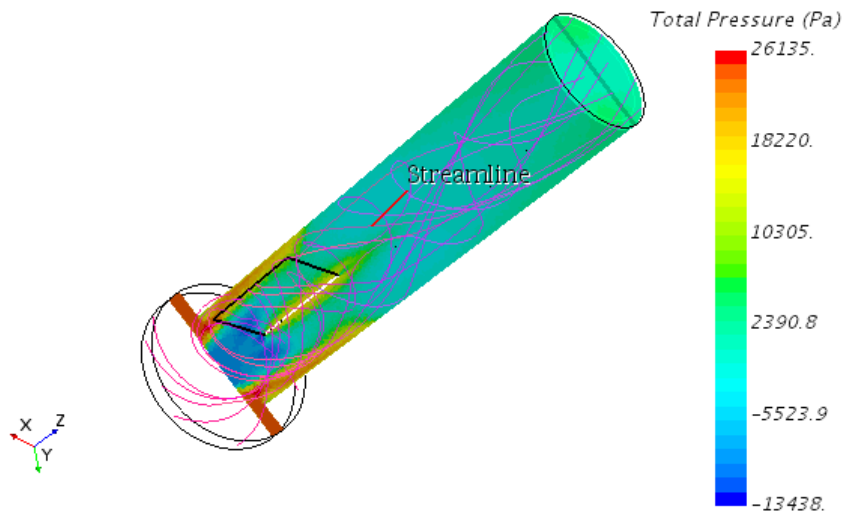
Figure 31: The scalar scene for the total pressure for the design 1.0

The figure 32 shows a detailed look at the zone where the plate's influence is preponderant.
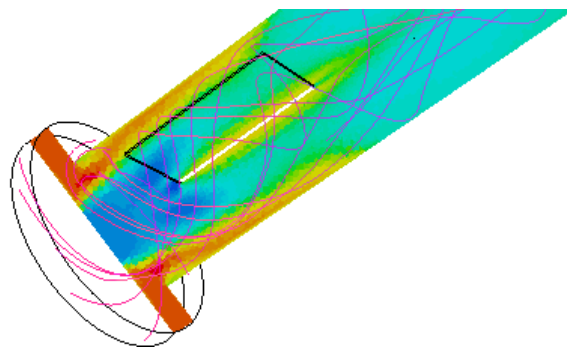
Figure 32: A detailed view of the streamlines in the crucial zone

In both figures, it can be clearly seen how the plate severely alters the swirl motion, making the swirl much less uniform and constant, and, although it can still be observed that after leaving the plate's zone the flow still has an important tangential component, the swirl becomes much more turbulent and chaotic. An immediate conclusion is that it is indispensable to develop this design and to contrive numerous variations, in order to optimize the results. Regarding the pressure distribution, it can be seen that it differs conspicuously from the one from the figure 21. Due to the presence of the plate in the

central region of the main cylinder, there is no longer a drastically low-pressure zone in the axis of the main duct.

The numerical results for the idea1.0, obtained after reaching convergence of the design, are shown in the table of the figure 33. Comparison with the initial (non-stator) design is included.

Parameter of interest	Value	Improvement of the design
Δ Static pressure	21.682 (Pa)	-14,61%
Δ Total pressure	22.208 (Pa)	3,80%
Tangential velocity (surface averaged)	25,38 (m/s)	77,63%

Figure 33: Results for the first proposed solution

It can be noticed, that the tangential velocity in the surface averaged circumference, is reduced in almost 78 per cent with respect to the initial problem, and in 71 per cent with respect to the basic stator design. The total pressure drop is not slightly less than in the initial geometry, however the static pressure drop has increased in almost 15 per cent. Nevertheless, the total pressure drop is much more crucial in this problem, and both parameters are highly supplementary towards the swirl reduction aspect, as it has been stated in the chapter 1.1 of the project. That is why, this concept proved to be highly promising, making it evident that it had a great potential in the swirl reduction procedure and required the designing of several variations, in order to select the most appropriate one.

The figure 34 illustrates the next approach, the idea1.1.

Figure 34: Design 1.1 - two perpendicular plates

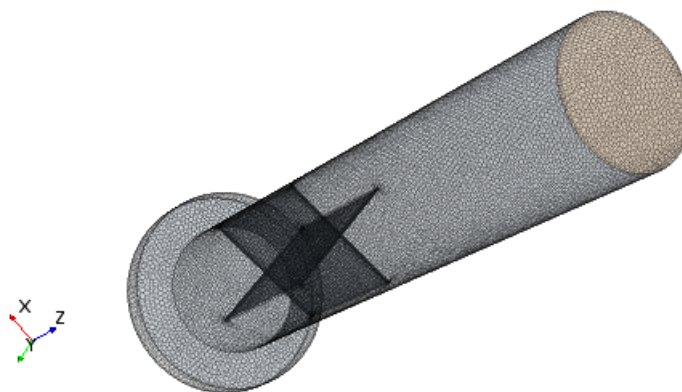In this case, there are two perpendicular plates that divide the flow into four segments upon its entrance into the plates' zone. This way, a very simple grid is already created. In the section 4.2 a detailed study of this idea's mesh independence will be explained.

4.2 Mesh independence study for the idea 1.1

Any CFD simulation must always have a detailed analysis of the mesh independence. This means, that a priori, it is impossible to know exactly what kind of mesh should be applied and to what extent it must be refined. Thereby, several simulations must be performed with different degree of mesh refinement, until the point where the numerical results for all the magnitudes remain practically constant. Only then, it will be assumed that the mesh is appropriate for this design.

For the idea 1.1, six cases were run, with different mesh refinement. Not only was the base size changed, but also several *customized mesh values*. A customized mesh is a meshing selected by the CFD user in order to refine some specific zone of the body, according to its size and to the complexity of the phenomena that will take place nearby that zone. For the idea 1.1, two customized meshes were created. The figure 35 shows the faces of the grid parallel to the longitudinal axis of the main cylinder. These faces were named "Internal walls 1". The figure 36 show the grid's faces perpendicular to the longitudinal axis of the duct, named "Internal faces 2", as it can be observed in both figures.
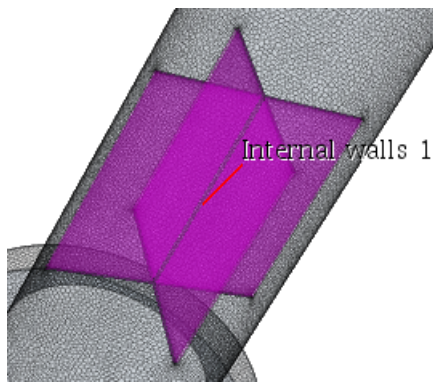
Figure 35: Internal walls 1
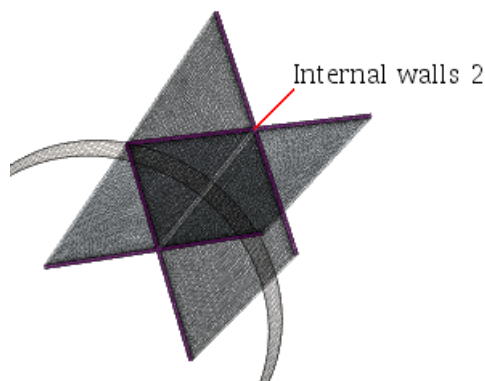
Figure 36: Internal walls 2

In order to customize these zones, two *surface controls* are created in the *automated mesh* option of Star CCM+. For each surface control, a *target* and a *minimum meshing size* were selected. All the studied body will have a base size, which is a selected value of each cell that will constitute the whole mesh of the geometry. A target size is the basic cell's percentage that will be chosen as the basic size for a particular part. A minimum size is also the basic cell's percentage, that will be selected in order to set the minimum allowed cell size for the meshing in a particular zone. As it can be noticed, due to a much smaller size of the internal walls 2 in comparison to the internal walls 1, the surface controls will be considerably more restricted in order to capture in detail the phenomena that occur in the proximity of these faces.

In order to select the appropriate meshing values, six simulations were run, setting an arbitrary, yet coherent percentage of the base size for both surface controls, and reducing progressively the base size. The first two attempts were purposely excessively big in order to give an overall idea of how the correct results should look. This is something that ought to be done in any mesh independence study. The most important parameter that will be compared is the meshing *cell number*, that is to say, the total number of cells created by the simulation in the meshing process. In this study, the target surface size of the internal walls 1 was set as 75 per cent of the base size; the minimum surface size

was set as 16 per cent of the base size. For the internal walls 2, these values were set as 16 and 12 per cent, respectively. The table on the figure 37 shows the summary of the mesh independence study.

Attempts	Base size (m)	Cell number	Tangential velocity (m/s)	Error tangential velocity	Delta p (Pa)	Error delta p
1	0,012	30500	2,99	0,5284	22409	0,0162
2	0,007	80150	5,16	0,1861	21887	0,0074
3	0,005	229000	6,02	0,0505	22053	0,0001
4	0,0045	346000	5,28	0,1672	22250	0,0090
5	0,004	497000	5,64	0,1104	22132	0,0037
6	0,0035	708000	6,34	0,0000	22051	0,0000

Figure 37: Mesh independence study results

It can be seen like, as stated before, the base size of the two first attempts is indeed considerably different from the rest and the total cell number for these two attempts is several times smaller than in the other cases. As can be deduced from the table, the values for the tangential velocity and for the static pressure difference are almost identical for the third and sixth attempt. In the columns corresponding to the relative error of all the attempts for these two variables, in relation to the last, sixth attempt, it can be noticed that the errors are very small in the last simulations; especially the difference between the third and the sixth attempt is inconspicuous.

The figure 38 is the representation of the tangential velocity in the derived part of the circumference intersecting the outlet, averaged along the whole circumference, against the number of cells in the generated volume mesh. It can be seen as, indeed, the third value is almost identical to the sixth one.
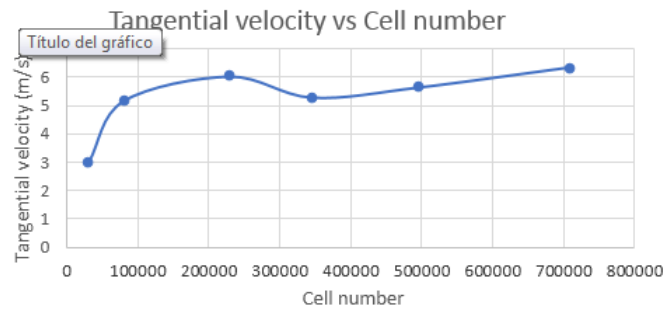
Figure 38: Variation of the tangential velocity with the increment of the cell number

The figure 39 is the representation of the static pressure drop against the total number of cells in the volume mesh.

As well as in the previous case, it can be also noticed as starting from the third attempt, the values become very similar and there is almost a repetition between the third and the sixth attempts' values. This means that mesh independence can be assumed and that there is no real need for further attempts, since the differences in the two most pertinent variables are very small. The attempt 3 is chosen as the one representing veraciously the phenomena present in the fluid volume, since it holds a very high similitude to the sixth attempt, which, in theory, is the most precise of all, yet it has less than a half of the cells in its volume mesh, which accelerates tremendously the calculations.

It is primordial to always bear in mind that in CFD it is indispensable to remember the *quid pro quo* rule, that is to say, the computational cost is something preponderant and it is necessary to minimize it as much as possible, without affecting too much the precision and exactness of the results.
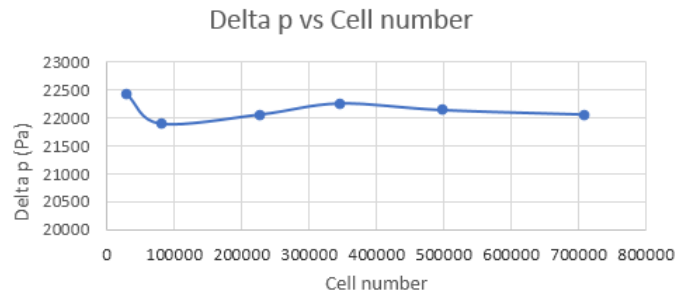
Figure 39: Variation of the static pressure drop with the increment of the cell number

The future designs of the chapter 4 will be analogical to the idea 1.1, however the number and the configuration of the plates forming the grid will vary. That is to say, the meshing assumptions can be identical to the ones studied in here.

4.3   The parametric study of the number of plates in the grid

It could be observed in the section 4.2 that the idea 1.1, involving two perpendicular plates is much more effective than the one with just one plate, i.e. the idea 1.0. The next two designs involve the augmentation in numbers of plates in the geometry, with respectively three and four plates, perpendicular to one another. The figure 40 represents the idea 1.2, and the figure 41, the idea 1.3. The meshing has been set as transparent in order to enable the complete view of the interior plates.
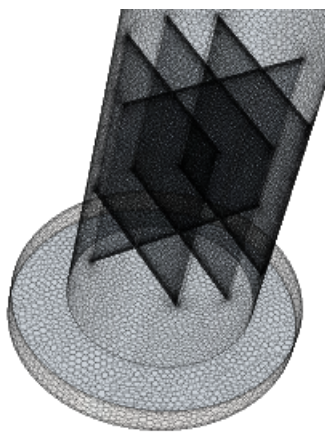
Figure 40: The design 1.2
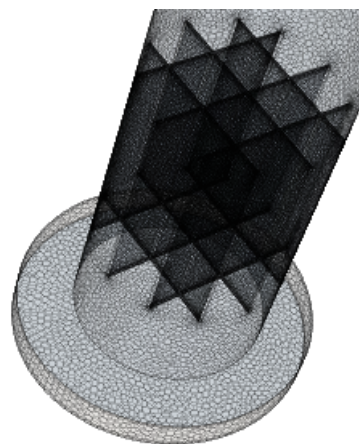
Figure 41: The design 1.3

It can be seen in both figure that the idea 1.3 forms a full grid that divides the flow in 16 different segments. It is a strong analogy to a honeycomb. The conceptual idea

consists in altering the flow so far that the initial boundary conditions become utterly irrelevant upon exiting the grid.

The figure 42 shows the streamlines for the geometry 1.3. It can be observed how the conceptual ideas are indeed valid. The flow enters through the inlet in a helicoidal way and forms a swirl motion. Consequently, it enters the grid and separates into 16 parts, that join together upon exiting the grid. At that point, the inlet conditions are no longer relevant and the streamlines form a relatively uniform and laminar movement, with almost no swirl whatsoever.
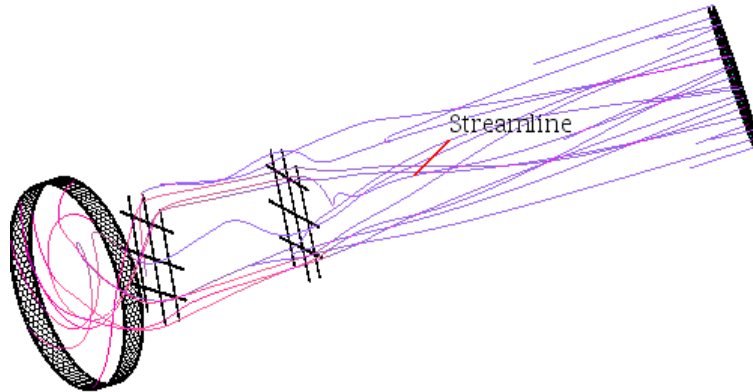

Figure 42: Streamlines for the idea 1.3

The table on the figure 43 summarizes the results for this parametric study.

Ideas	Tangential velocity (m/s)	Delta p (Pa)	Total pressure inlet (Pa)	Total pressure outlet (Pa)	Delta total p (Pa)
1.0	25,38	21682	24120	1912	22208
1.1	6,02	22053	23615	1469	22146
1.2	-5,88	21488	22937	1434	21503
1.3	1,53	21083	22558	1442	21116

Figure 43: Results for the parametric study of the number of plates

In the first place, it must be noticed that the idea 1.0 includes the mesh settings concluded after the mesh independence study, that is to say, this idea was simulated using the appropriate meshing refinement, described in the section 4.2.

It can be observed that the tangential velocity is almost null in the last of the four designs, and that the pressure drops, both static and total, are less than in all the other three geometries. Nonetheless, as a matter of fact, all the last three geometries present very low values of swirl, thereby it can be concluded already at this point, that the swirl has been practically eradicated, also reducing the pressure difference between the inlet and the outlet.

Figures 44 and 45 show a graphical plot of the two most important parameters in this problem.

It can be seen as in the design 1.2 the average tangential velocity at the circumference-derived part is less than zero, hence a reversed flow is present at the outlet. This is the best sign that even the geometry 1.2 eradicates the swirl, nevertheless, this geometry creates considerable flow turbulence upon exiting the grid, and thereby the flow is not

as laminar as in the geometry 1.3. That is why, the absolute value of the tangential velocity in the studied derived part is minimum in the four-plate grid: it acts upon the flow so intensely that not only does it break the swirl completely, but also minimizes the turbulence. That is why, this design, 1.3, is selected as the optimum of all these cases.
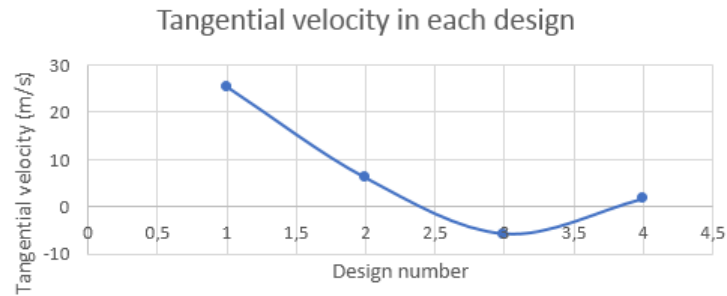
Figure 44: Variation of the tangential velocity from the first design (1.0) to the fourth one (1.3)
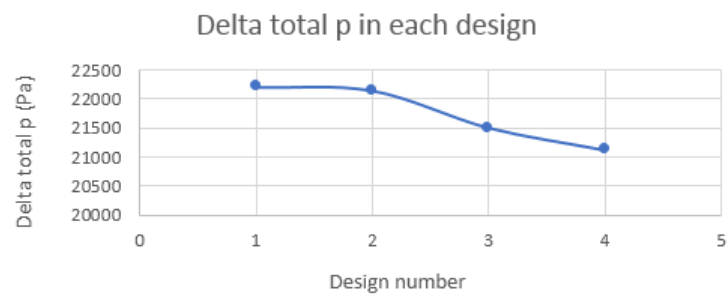
Figure 45: Variation of the total pressure drop from the first design (1.0) to the fourth one (1.3)

Although the effect on the swirl reduction of this geometries is astounding, and the pressure does not augment with respect to the initial design, it is still possible to reduce the pressure drop much more. The current improvement of the delta total pressure has the value of 8,53 per cent. If the exclusive objective of this problem was to minimize the swirl, the thesis could be assumed as finished, since the tangential velocity at the reference circumference at the outlet has been reduced from $113,47$ to $1,53 m/s$. That is to say, a reduction of 98,65 per cent has been accomplished. However, the pressure drop is not optimized yet, therefore all the future designs will aim at this purpose.

As a last mention, it must always be kept in mind that this is an engineering problem, studied from a pragmatic, industrial perspective, thereby the simplicity and cost of the design is always a preponderant factor. This optimum design should be implemented in practice, using actual mechanical tools and materials. It is of course possible to simulate a grid with five or more plates, and probably observe some pressure improvements, however at that point it might become too impractical for the actual technological purposes. That is why, other approaches shall be pondered.

46

4.4 The parametric study of the location of the grid

The next stage of the project consisted in performing the parametric study of the location of the grid, based on the design 1.3, with a four-plate grid. The optimum configuration was selected, after designing six different geometries, varying the grid's location along the main cylinder. The initial design, 1.3, had the base of the grid situated 0,092 m from the very base of the body. One design with a lower grid was created, and four with the grid located higher than in the design 1.3. The figure 46 illustrates the geometry 2.5, with its grid situated 0,35 m high.
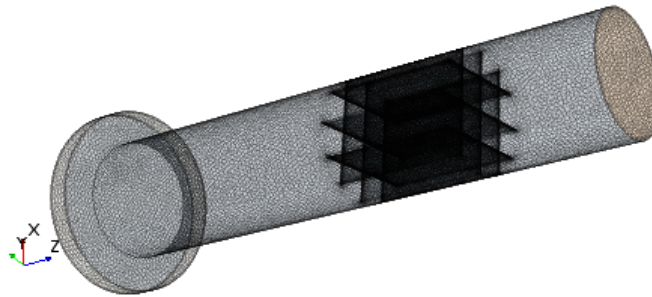
Figure 46: The design 2.5, the grid situated 0,35 m high

The figure 47 illustrates the result of this simulation on the flow's streamlines.

Figure 47: Streamlines view for the design 2.5

The effect on the streamlines can be seen as visually the same as in the figure 42, with the same grid-influence mechanism, thereby in order to actually compare its effect, it is inevitable to run the appropriate reports and plots. The results are shown in the table of the figure 48.

It becomes evident that the lower the grid is located, the bigger is its influence on the swirl reduction. Apart from the exception in the design 2.3, which doesn't follow this rule, however, the general tendency is more or less clear. It may be this way, since the lower the grid is, the more space the flow will have after exiting the grid to dissipate the turbulent energy and become more laminar and smooth. Regarding the total pressure drop, the value is much more favorable for the lowest locations of the grid, in this case, without any exception whatsoever. In the figure 21, it can be observed that the bigger pressure drop inside the main duct occurs right at its lowest zone, thereby filling the geometry with a solid set of parts, such as a grid in this case, may eliminate certain

47

recirculation zones in the flow, thus reducing the pressure drop.

Ideas	Location of the grid's lowest point (from the very base) (m)	Tangential velocity (m/s)	Delta p (Pa)	Delta total p (Pa)
2.1	0,03	0,64	19264	19306
2.2 (1.3)	0,092	1,53	21083	21116
2.3	0,16	0,88	21643	21695
2.4	0,25	1,92	22405	22476
2.5	0,35	3,64	23609	23947
2.6	0,45	4,82	24244	24774

Figure 48: Results for the parametric study of the grid's location

The figure 49 illustrates the plot for the tangential velocity in the circumference of the outlet, defined equally for all the designs of this project.
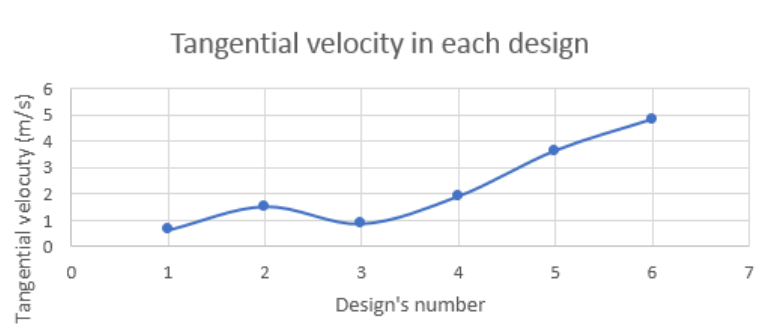
Figure 49: Variation of the tangential velocity with the grid's location

The figure 50 shows the plot for the total pressure drops in all six designs.
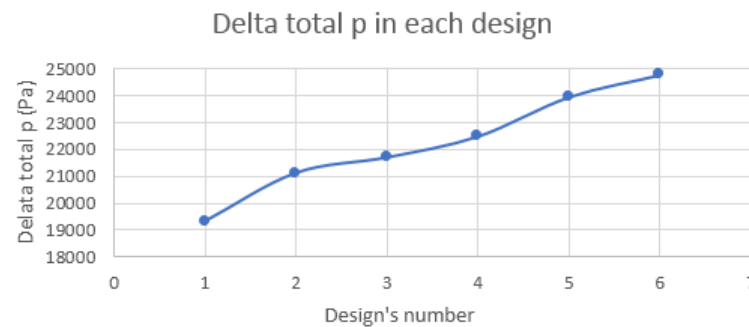
Figure 50: Variation of the total pressure drop with the grid's location

All in all, it can be concluded that by both criteria, the design 2.1 is the optimal, since it minimizes the swirl, as well as the static and total pressure drop. From the swirl reduction point of view, practically all the designs are acceptable, thereby that should be kept in mind when performing the actual manufacturing of the construction, if certain designs are not feasible or if some additional component must be installed in the lower part of the duct. Notwithstanding, from the pressure drop point of view, there is a substantial difference between these six designs, since the two last concepts increase delta p, whereas the design 2.1 reduces it in 16,37 per cent, being definitely the most appropriate design so far.

4.5   The parametric study of the grid's height

In this step, a parametric study was performed, in which the height of the grid along the longitudinal axis of the main cylinder was changed from 5 mm to 25 mm, in five different designs. The starting point was the location established in the chapter 4.3 as optimum, i.e. the design 2.1. The table of the figure 51 shows the results for the five geometries.

Ideas	Height of the grid (m)	Tangential velocity (m/s)	Delta p (Pa)	Total pressure inlet (Pa)	Total pressure outlet (Pa)	Delta total p (Pa)
3.1	0,05	-6,1	19812	21334	1458	19876
3.2	0,1	-4,03	19448	20938	1444	19494
3.3 (equal to 2.1)	0,15	0,64	19264	20740	1434	19306
3.4	0,2	1,8	19151	20613	1430	19183
3.5	0,25	2,02	19238	20694	1428	19266

Figure 51: Results for the parametric study of the grid's height

It can be seen that all the design present very low tangential velocities in the reference derived part at the outlet of the body, and the first two of them have reversed flow in that zone. The plot for the tangential velocities is represented on the figure 52.

Figure 52: Variation of the tangential velocity with each design

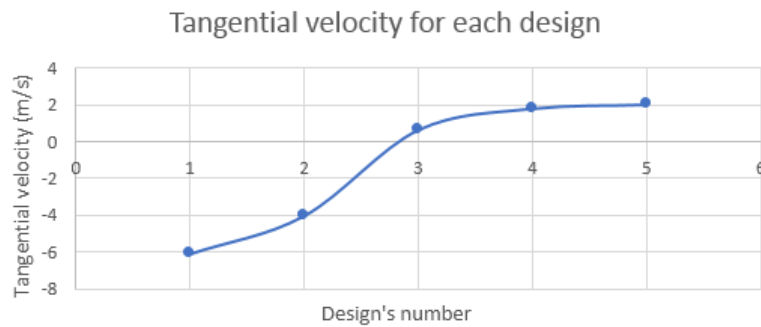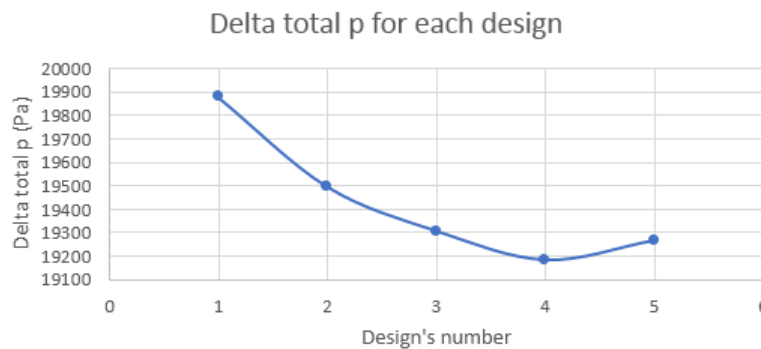Figure 53: Variation of the total pressure drop with each design

The tendency is not clearly marked, however, it looks like the optimum point corresponds to the designs 3.3 and 3.4. The optimum should be the point with the lowest absolute

value of tangential velocity, since not only will the swirl be eradicated in that case, but also the flow will be much more laminar and smooth.

Regarding the pressure drop, all the designs present relatively acceptable delta of the static and total pressure, being substantially improved in comparison to the initial geometry. The plot for the pressure drop is shown on the figure 53.

The minimum total pressure drop corresponds to the design 3.4. Also, the static pressure has its minimum drop in this design. Both the designs 3.3 and 3.4 present very acceptable results for both variables, however, since in this parametric study, it is attempted to minimize the pressure as much as possible, the design 3.4 will be chosen as the most appropriate, considering all the aspects analyzed in this chapter.

4.6 Analysis of the optimum desingt

After having performed three parametric studies of the grid concept, it was determined that the most adequate design is 3.4. The figure 54 shows an insight of this geometry, after having set the mesh as transparent, in order to visualize the interior.
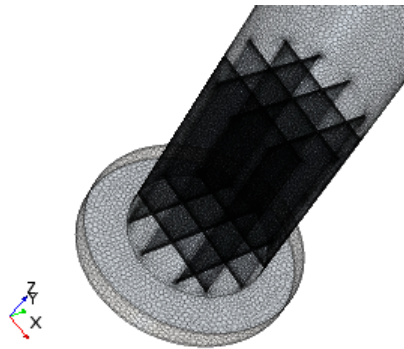
Figure 54: The optimum geometry view - meshing set as transparent

Firstly, it has been determined that a four-plate grid is optimal taking into account the effect on the relevant variables and the relative simplicity of the geometry. Secondly, it was established that the lower the axial location of the grid is, the better the effect on the swirl reduction and the pressure drop reduction is. Eventually, the most favorable grid's height was selected.

Not only is this geometry the most effective of all the studied in the chapter 4, but it is also the most favorable of all the geometries studied and simulated throughout the development of this thesis, as it will be seen in the chapters 5 and 6. It combines a practically full eradication of the swirl, which was the main purpose of this task, with a considerable total pressure drop reduction. The table from the figure 55 compares the results for this final design to the initial geometry of the problem.

It can be indeed observed how great an improvement in the swirl reduction has been accomplished, and additionally, that the total pressure drop is also considerably lower. Only the static pressure drop is slightly bigger, nonetheless, this difference is inconspicuous and this parameter is less pertinent to the problem than the total pressure drop.

The figure 56 shows the design's scalar scene with a clear view at the flow streamlines.

Variable of interest	The final design's value	Improvement comparing to the initial geometry
Tangential velocity (surface averaged on the derived part)	1,8 m/s	98,41%
Δ Total pressure	19.183 Pa	16,89
Δ Static pressure	19.151 Pa	-1,23%

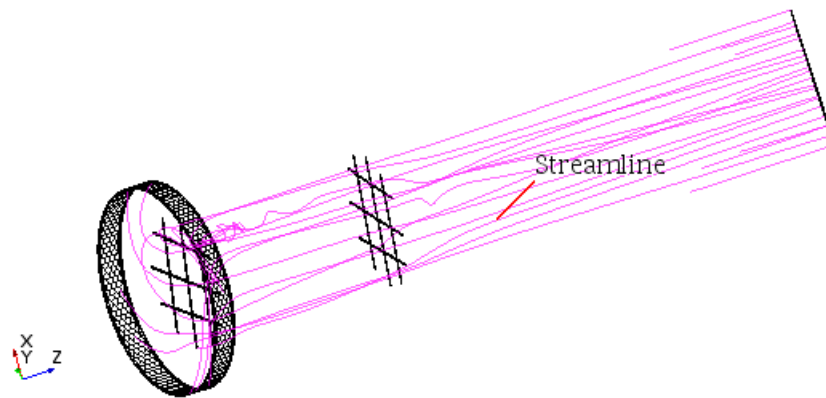Figure 55: Parameters for the optimum design

Figure 56: Streamlines view for the optimum design

In this figure, it is perspicuous that the grid makes the swirl vanish and it becomes practically laminar at the end of the duct, near the outlet. On the other hand, the figure 57 illustrates the scalar scene with the distribution of the tangential velocity over the outlet of the body. The axes have been confined in such way that the minimum value shown is -5 m/s and the maximum is 5 m/s, as can be observed. This way, it is utterly clear that the tangential velocity is very small in the whole of the outlet.

Finally, the figure 58 represents the scalar scene of the distribution of the total pressure, over a derived part in form of a plane that contains all the longitudinal axis of the main cylinder. It can be noticed that the very strong gradients, that could be observed in the figure 21, on the initial geometry, totally disappeared, and that the total pressure distribution is now much more uniform. The grid, with a 20 cm of height and situated 3 cm over the very base of the body, fills, to a certain extent, the recirculation zones in the duct. Apart from that, the grid is divided into sixteen smaller segments, which make the flow uniform in all the transit throughout it; this also contributes to the pressure uniformization. Also, as it can be observed, there is no swirl whatsoever upon exiting the grid, thereby, there is no central zone with lower pressure by definition. That is why the pressure scalar scene is utterly different from the one in the figure 21.

A last emphasize pertaining to the final design of this chapter is that this design is far simpler and easier to construct industrially than the other geometries analyzed in this

project, and it's by far more inexpensive than all the designs based on a stator concept. Thanks to all its advantages, this design was chosen as the optimum method of the project for the reduction of the swirl.
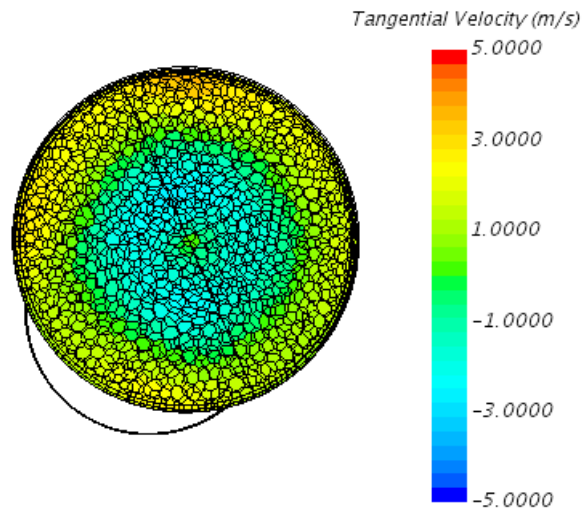

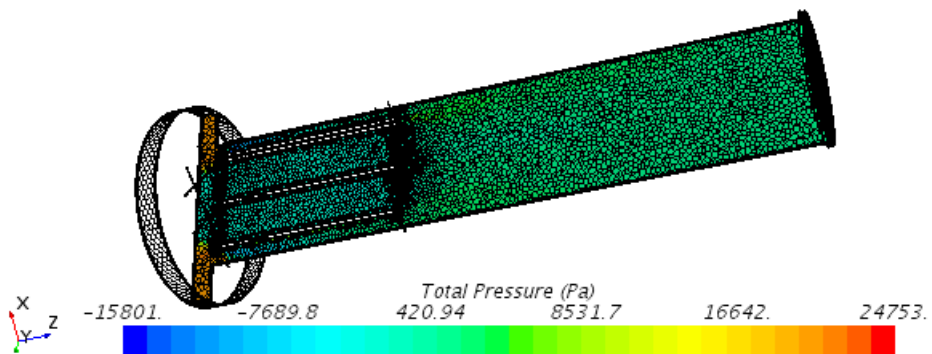Figure 57: Tangential velocity distribution over the outlet of the body

Figure 58: Scalar scene with the total pressure distribution for the optimum design

Chapter 5

5 Alternative solutions

It has already been seen in the chapter 4 that the grid solution provides fully satisfactory results for the swirl reduction and a considerable improvement in the aspect of the pressure drop. It also combines a relative manufacturing simplicity, which is a primordial issue in any engineering design.

In this chapter, numerous designs aimed at the swirl and pressure drop reduction will be implemented. Since the swirl is no longer a problem thanks to the grid designs, the main approach of the chapter 5 will be the pressure drop minimization. 15 designs have been implemented throughout this chapter, achieving interesting and pertinent conclusions. Nonetheless, as it was stated at the end of the chapter 4, the optimum design in the whole project is still the design 3.4, taking under consideration all the variables of interest involved.

5.1 Recirculation zones approach

It was seen on the figure 21, mentioned several times in this thesis, that the initial geometry presents a flagrant recirculation zone in the interior of the swirl, because of the swirl's helicoidal motion. Something very similar in nature is the example of the wind forming a cyclone or a tornado, where the interior presents a very low pressure, with almost no fluid movement whatsoever. A logical approach will be then to attempt to fill the interior of the swirl in the main duct of the body in different ways.

In this section, different designs will be implemented, presenting several forms of filling the recirculation zones of lower pressure, as well as combining it with the grid geometry, in order to intend to accomplish a synergy in the design. All the designs aimed at this purpose will be successively explained, as well as a summary with the results will be exposed in form of table at the end of the section 5.1, with conclusions for the section 5.1.

Design 4.1

The first design consisted in creating a body inside the main duct, at its bottom, that would fill the recirculation zone and reduce the pressure drop. The figure 59 illustrates the design.

This interior body is comprised by a cylinder, with a 37-mm radius and a 200-mm height, and a cone located onto it, with a 50-mm height. The figure 60 illustrates the scalar scene with the flow streamlines and the total pressure distribution, which is the main parameter of interest in the section 5.1.

It can be noticed that the internal recirculation zone does not disappear, just moves upward the main duct. The total pressure drop between the inlet and the outlet of the whole body however, does decrease, in comparison to the initial geometry: 23.084 comparing to 21.904 Pa, meaning an improvement of 5,11 per cent. The swirl motion is not affected, since this design does not implement any mechanism that would reduce it. In fact, the tangential velocity in the derived part of the outlet is now almost 1 m/s

higher, reaching 114,16 m/s. This design allowed to see that filling the recirculation zone may contribute to the pressure drop reduction, however it has to be necessarily combined with a swirl reduction geometry, such as the beforementioned grid. This will be the objective of the next designs.
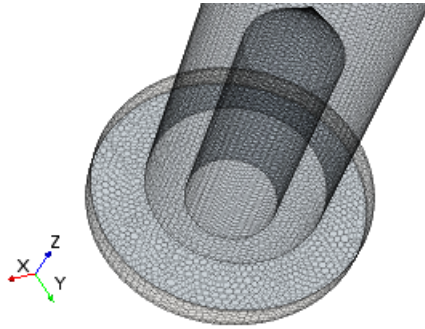

Figure 59: The design 4.1 with a transparent meshing
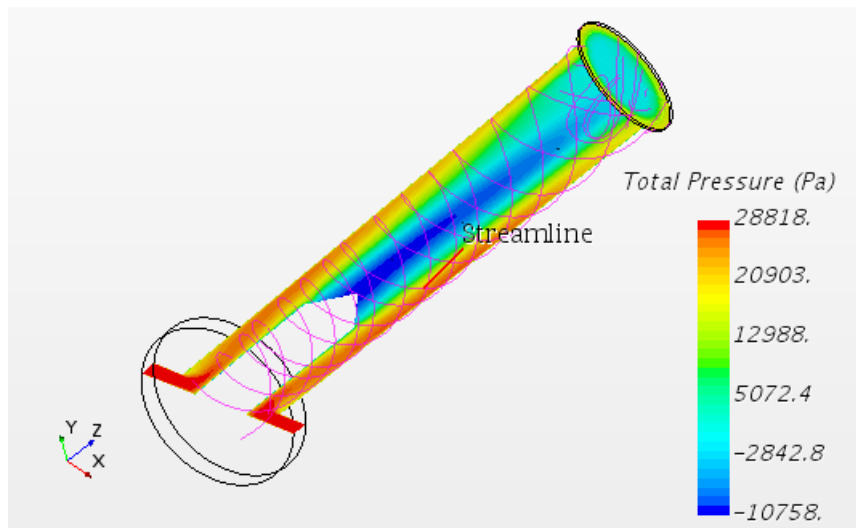
Figure 60: Scalar scene with streamlines for the design 4.1

Designs 4.2 and 4.3

The design 4.2 is the combination of the geometries 4.1 with the grid located at 0,25 m from the bottom with a height of 0,15 m, that is to say, with the geometry 2.4, studied in the chapter 4.4 of this thesis. The figure 61 is the scalar scene representing the streamlines and the pressure distribution throughout the duct. It can be observed how this combined design implements both concepts deeply analyzed in this project, i.e. the flow division into several segments that reduces the swirl, and the recirculation zone filling with an internal body. It can be seen that the total pressure distribution along the main duct is relatively homogeneous, since the recirculation zone inside the duct is filled both by the cylinder with cone and by the grid. Regarding the swirl configuration, it can be seen, that it is almost eradicated, due to the action of the grid.

The reports show that the tangential velocity at the reference derived part is now 3,34 m/s, which is slightly more than the 1,92 m/s present in the design 2.4. Nevertheless,

these velocities are so small in comparison to the initial value of 113,47 m/s, that it can be still assumed that the swirl has been eradicated.
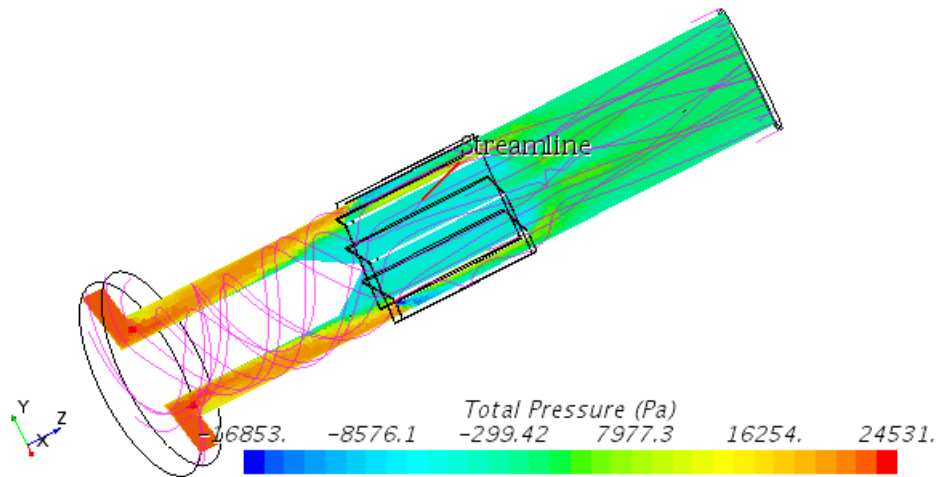
Figure 61: Scalar scene with streamlines for the design 4.2

The total pressure drop has now the value of 21.210 Pa, which shows an improvement with respect to the geometry 2.4 with the value of 22.476 Pa. It is thus corroborated that the recirculation flow filling is indeed a viable way of improving the total pressure drop in comparison to applying the grid alone, at least for this grid configuration of the design 2.4.

The next design is the 4.3, when it was intended to modify the internal filling form in order to choose the most favorable one. The figure 62 shows the new geometry.

Figure 62: The design 4.3 with a transparent meshing

This time the cylinder is much shorter, 0,1 m, and the cone is much sharper, having a height of 0,14 m. The conceptual guess is that this much sharper form might cause the progressive swirl adaptation to the internal filling, reducing this way the pressure

gradients more effectively. The figure 63 illustrates the scalar scene of total pressure delta with the streamlines for this geometry.

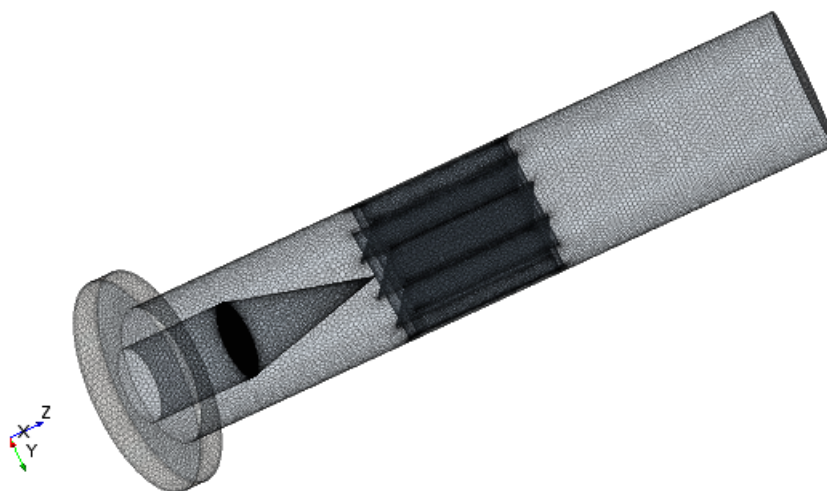A priori, no definitive conclusions can be extracted from the mere visual analysis of the scene. The reports however, show that there is no considerable difference in comparison to the design 4.2; in fact, the result is slightly inferior from the pressure drop point of view.
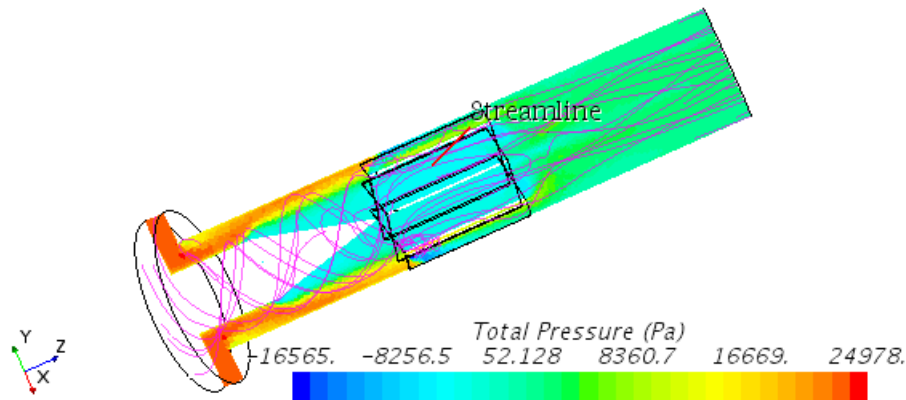

Figure 63: Scalar scene with streamlines for the design 4.3

The tangential velocity of the reference derived part is now 2,98 m/s, which is a slight, yet inconspicuous improvement in this regard. Notwithstanding, the total pressure drop is now 21.696 Pa, which is slightly more than in the design 4.2. The conclusion should probably be that there is no significant influence of changing this way the form of the internal body, and leaving it as it was previously, is not a bad solution in comparison to this one.

Designs 4.4 and 4.5

The purpose of the next design is to check if the cone construction onto the internal cylinder is really necessary, since not building it would definitely simplify the manufacturing and, as it could be seen in the figures 61 and 63, the scalar scenes didn't show any actual influence of the cone structure on the flow. The figure 64 shows the geometry without a cone, with an internal cylinder of 0,2 m height. The grid is the same as in the design 2.4.

The figure 65 illustrates the scalar scene for this design. The parameter shown is as usual the total pressure distribution, since it is the most relevant parameter in the whole chapter 5 in the thesis hereof. The streamlines are also presented.

It can be observed that the flow's streamlines are almost identical to the ones in the geometry 4.2, which did have a cone on its cylinder. The same can be said about the pressure distribution. The reports show that the tangential velocity is now 3,36 m/s, which is exactly the same as the 3,34 in the design 4.2. The total pressure drop is 21.133 Pa, which also shows no practical difference whatever with respect to the design 4.2.

The overall conclusion for the design 4.4 is that it is the same to build the cone and not to build it. Thereby, with the purpose of simplicity, the cone should not be usually
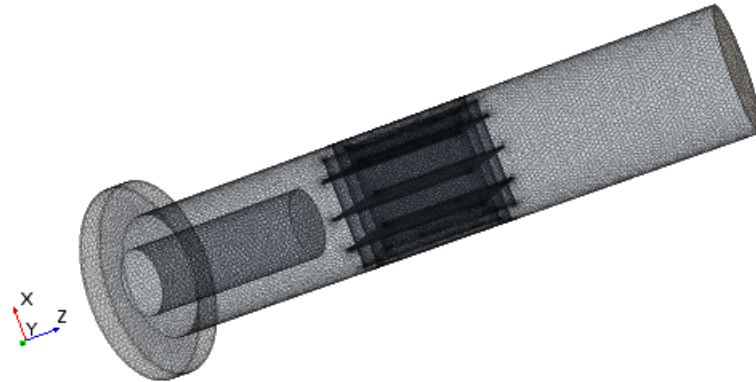
constructed.

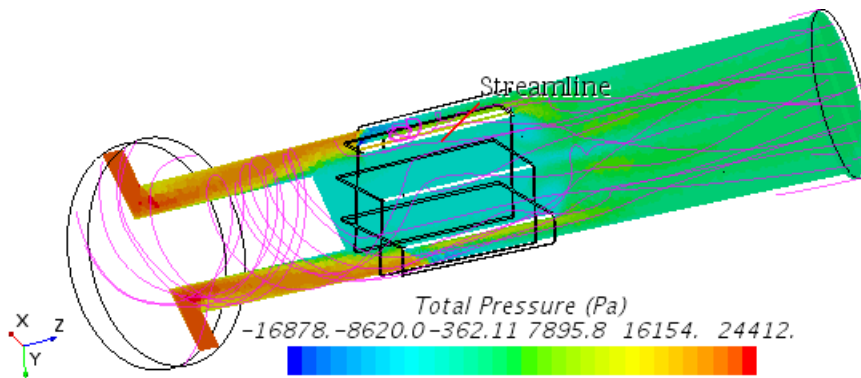Figure 64: The design 4.4 with a transparent meshing

Figure 65: Scalar scene with streamlines for the design 4.4

The design 4.5 locates the grid 0,45 m upon the very base of the body, as it was done in the design 2.6, and puts an internal cylinder with a 0,35-m height, this time. It was previously determined that the more the grid's location increases, the less the swirl be reduced. However, the idea of the geometry 4.5 is to see if increasing the internal filling significantly improves the effect on the pressure drop between the inlet and the outlet. The figure 66 shows the new design.

The figure 67 represents the scalar scene of the geometry, with the same settings as seen so far. The streamlines and the total pressure distribution visually look coherent to the ones in the design 4.4. The reports analysis shows that the tangential velocity is 7,15 m/s, which is more than the 4,82 m/s of the design 2.6, with this grid alone without the internal cylinder. The total pressure drop however, shows improvement with respect to the geometry 2.6, as it has now it has a value of 21.444 Pa, more than 3.000 Pa less than the 24.774 Pa of the geometry 2.6. This value is still bigger than in the geometry 4.4, where the total pressure drop is 21.133 Pa, as seen in this section. That is so because, in spite of the fact that the internal cylinder now reduces better the pressure drop than in the geometry 4.4, the grid from the geometry 4.4 contributes much better to the delta p reduction than the one from the current design.

The conclusion for the design 4.5 is that, all in all, it is not propitious for the problem's

solution to locate the grid this high, even if the internal cylinder is now able to fill better the recirculation zone of the whole duct.
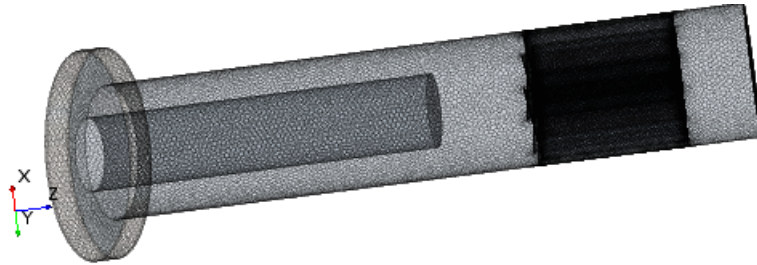
Figure 66: The design 4.5
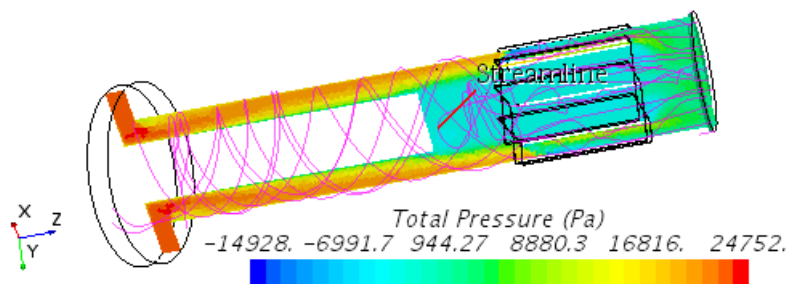
Figure 67: Scalar scene with streamlines for the design 4.5

Designs 4.6 and 4.7

The next two designs, the last ones for the section 5.1, will try to fill the recirculation flow with a cylinder and a cone, this time extruded inside the internal cylinder itself. The initial guess is that, although constructing the cone inside the cylinder will add an additional recirculation zone to the body, this additional zone might absorb part of the swirl flow, helping in its reduction, which might improve the overall results for the problem. The figure 68 illustrates this new design.

Figure 68: The design 4.6

The figure 69 on the other hand is the scalar scene for this geometry, with the same

settings as before. At the first glance, there is no influence upon the streamlines' structure. The tangential velocity of the report is 3,25 m/s, which is exactly the same as in the internal cylinder without any cone inside it. The total pressure drop is 21.080 Pa, which also shows only an inconspicuous improvement with respect to the geometry 4.4.
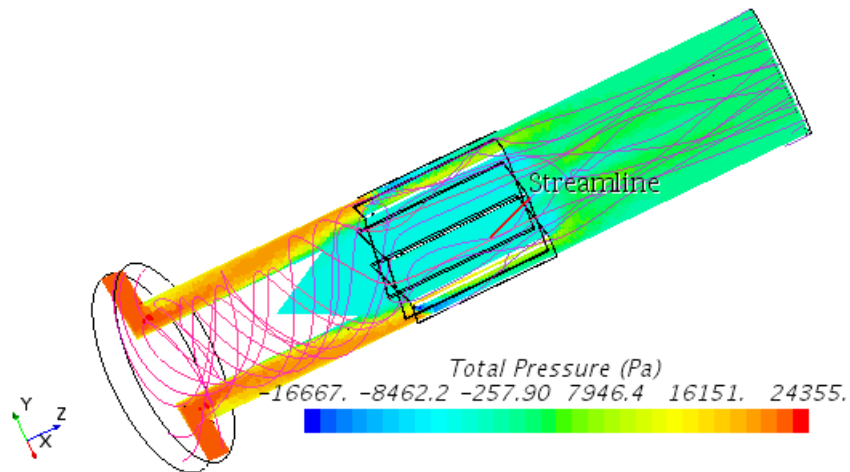
Figure 69: Scalar scene with streamlines for the design 4.6

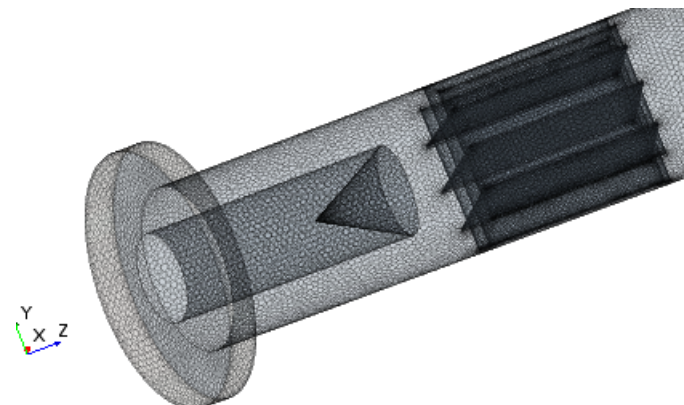The conclusion for the design 4.6 is that the internal cone in this form doesn't change the flow, thereby for the sake of simplicity, it should not be included in the design.

Finally, the design 4.7 attempts at modifying the cone inside the internal cylinder, making it much more pronounced and large. In fact, it is no longer a cone, but a revolution body created via a spline-sketch in the CAD option of Star CCM+. The figure 70 shows this design.
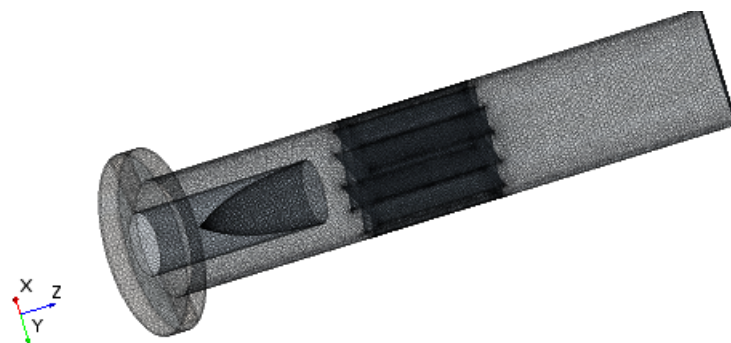
Figure 70: The design 4.7

The design's purpose is to check whether this time the cone inside the internal cylinder has some tangible impact upon the flow. The figure 71 illustrates the scalar scene with the streamlines.

The report's value for the tangential velocity is now 3,32 m/s, still having no difference with respect to the design without a cone inside the internal cylinder, that is to say, to the design 4.4. The report's value for the total pressure drop is 21.107 Pa, which makes no difference either, with respect to the design 4.4.

The conclusion for the both last designs is that constructions inside the internal cylinder don't change the swirl's behavior nor tendencies, therefore they should not be implemented into the manufacturing process.
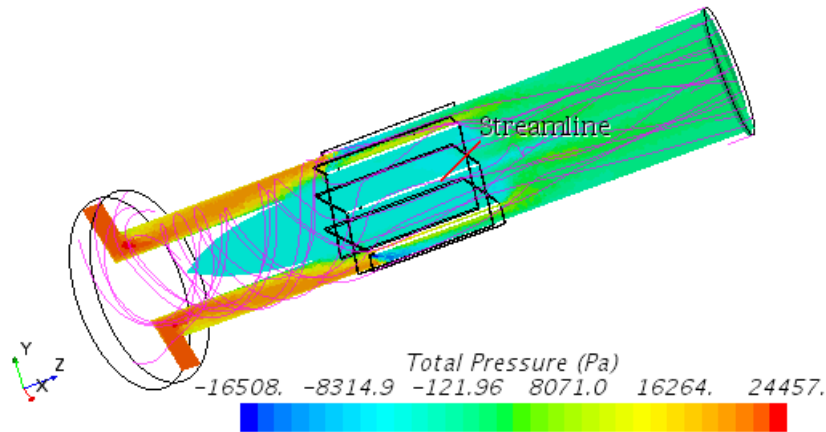
Figure 71: Scalar scene with streamlines for the design 4.6

The table on the figure 72 summarizes the results for all the seven designs studied in this section.

Design's number	Cylinder's height (m)	Cone's height (m)	Tangential velocity (m/s)	Static pressure drop (Pa)	Total presure drop (Pa)
4.1	0,2	0,05	114,16	17624	21904
4.2	0,195	0,05	3,34	21150	21210
4.3	0,1	0,14	2,98	21637	21696
4.4	0,195	0	3,36	21071	21133
4.5	0,35	0	7,15	20908	21444
4.6	0,17	0,7 (downwards)	3,25	21014	21080
4.7	0,17	(a spline)	3,32	21025	21107

Figure 72: Results for all the designs considering recirculation zones filling

It can be concluded that the recirculation zone filling shows certain improvements in comparison to the basic grid design. The internal geometry should not contain any cone, neither onto nor inside the internal cylinder, since the cylinder alone shows the same results and it's simpler to manufacture. The internal cylinder's height should not be too big, since it is more convenient to place the grid as low as possible, as it has been seen in this section. The design 4.4 is thereby the most effective from the seven, taking into account the overall aspects.

Nevertheless, it can be seen, that the best of the seven designs is still inferior to the grid alone, placing in the appropriate location, i.e. to the design 3.4. The tangential velocity differences are inconspicuous, however, the total pressure drop accomplished in the design 3.4 was 19.183 Pa, 9,23 per cent better than in the design 4.4. The problem with the filling recirculation zone designs is that, due to these zones' distribution, the internal fillings must be located at the bottom of the main duct. Nonetheless, the

optimum grid location was also shown to be as low as possible, thereby both design are mutually exclusive. They are both good methods of resolving the problem presented at the beginning of the thesis hereof, however, the best design is still the one containing only the grid inside the main duct. Besides, the grid-alone construction is, by definition, simpler and cheaper than a design implementing both the grid and the internal filling geometry.

5.2   Internal geometry with a "star-shaped" grid

In this section, it will be intended to combine the pressure recirculation filler with the grid into one single geometry. For this purpose, the grid will have a stellar shape, with its origin in form of the filler body. The point is to combine the concepts from the two previous approaches into a single one, and also, to eliminate the space between the internal body and the grid, present in the section 5.1's designs, since this space might contribute to certain pressure losses in the flow. The effects of such geometry will be analyzed and compared to the previous approaches. At the end of this section, all the results will be summarized in a table and the overall conclusions will be clarified.

Design 5.1

The first design of this section is based upon a short cylinder of 0,2 m height and a cone of 0,09 m placed onto it. The grid is embedded in the internal body with eight, 0,1 m - high plates. The figure 73 illustrates the design. The conceptual idea is that placing the internal body in the base of the main duct may reduce the pressure drop, since the parametric study of the grid location from the previous chapter showed that the grid should be located as low as possible.
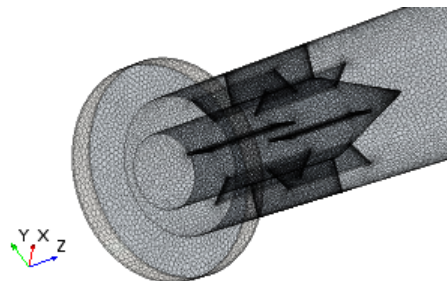
Figure 73: Design 5.1

The figure 74 presents the scalar scene of the previously commented characteristics, for this geometry.

It can be seen that the flow is relatively turbulent after exiting the grid. The tangential velocity report indicates a value of -4.87 m/s, meaning that there is a certain backflow in the outlet of the main duct. The swirl's magnitude is however small, which shows that the star-shaped grid is indeed effective.

Concerning the total pressure drop report, the outcome value is 20.954 Pa, being slightly higher than in the optimum design of the project, that is to say, the design 3,4. This means that the design didn't accomplish its original purpose of improving the pressure drop with respect to the geometry 3,4, however it is indeed a feasible alternative.
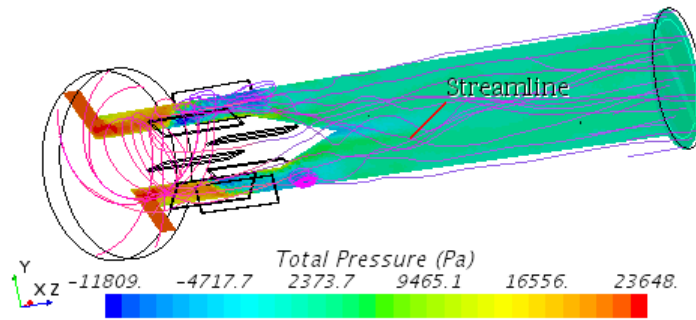
Figure 74: Scalar scene with streamlines for the design 5.1

Design 5.2

The figure 75 shows a variation of the geometry 5.1. It can be observed that the internal cylinder has been increased in height, to a new height of 0,552 m, in order to locate a cone on its surface. This design attempts at checking if the cylinder's height will influence the pressure drop.

Figure 75: Design 5.2

On the figure 76, the scalar scene of this design can be observed, with the total pressure distribution and streamlines included in the scene.

Figure 76: Scalar scene with streamlines for the design 5.2

At the first sight, the streamlines after leaving the grid become slightly turbulent and, looking closer at the cone region, it can be noticed that they adapt relatively well to the

cone shape. The report for the tangential velocity shows a result of 9 m/s. This means there is no backflow in the outlet and the tangential velocity is very small, although higher than in the design 3,4, the optimum design of the thesis. The total pressure drop report however, shows a value of 20.879 Pa, which is an improvement of almost 100 Pa with respect to the design 5.1. This shows a superiority of this design in comparison to the version 5.1 in the aspect of the pressure drop, which is the most important issue in the chapter 5.
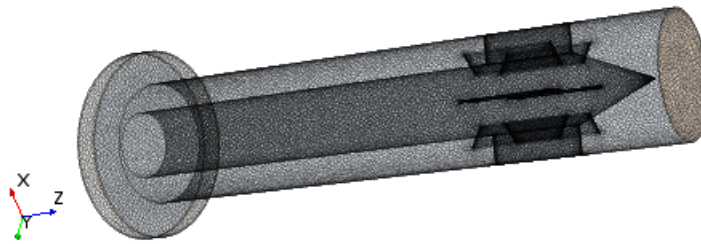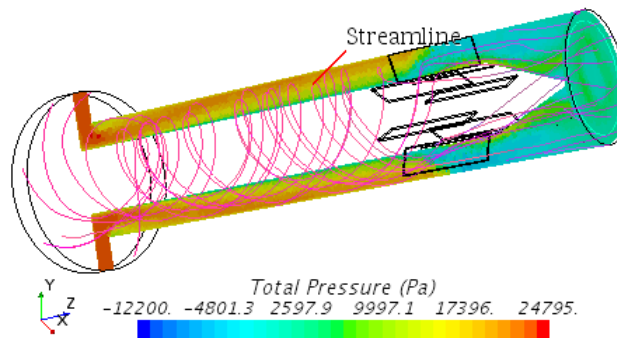
Design 5.3

The objective of this attempt is to vary the height of the plates forming the grid, decreasing them from 0,1 to 0,05 m, and to observe the differences. The so accomplished geometry is visualized on the figure 77.
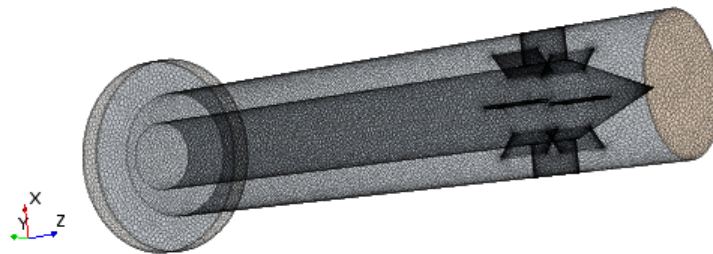
Figure 77: The design 5.3

The figure 78 on the other hand, shows the scalar scene for this design. A highly turbulent zone is observed in the cone vertex, near the outlet of the body. The report for the tangential velocity shows a value of 12,61 m/s, higher than in the previous two designs. The report for the total pressure drop shows a value of 21.406 Pa, which is more than in the design 5.2.
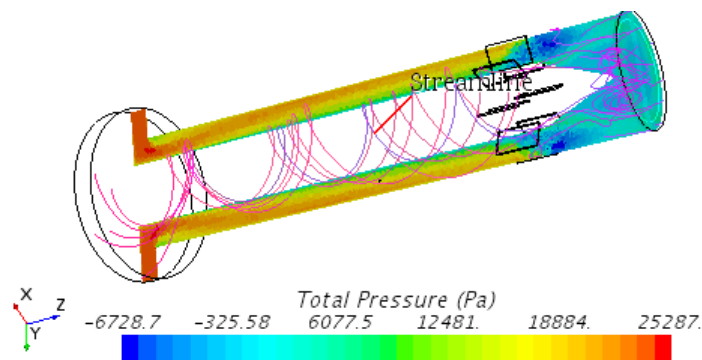
Figure 78: Scalar scene with streamlines for the design 5.3

All in all, the swirl improvement in this design is not satisfactory and the pressure drop improvement is not observable. This geometry is thereby not comparable to the ones analyzed so far. The height of the plates selected will remain being 0,1 m.

Design 5.4

This design will vary the version 5.2 in the number of plates forming the grid. It will be checked if the plates number should be indeed as high as possible, as it was deduced in the chapter 4. This design in here will have only four symmetrical plates, located in such way as shown on the figure 79.
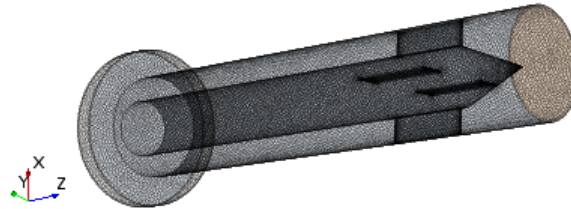
Figure 79: Design 5.4

The figure 80 shows the scalar scene for this design, with the total pressure distribution and the streamlines that illustrate the flow behavior.
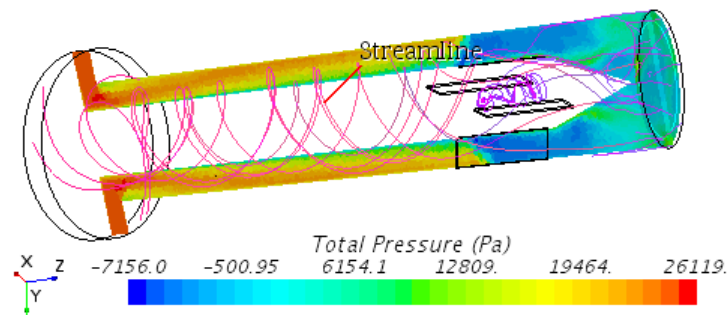
Figure 80: Scalar scene with streamlines for the design 5.4

It can be seen on the figure 80 that the grid's effect may not be as perspicuous upon the flow's streamlines as in the design 5.2. The report for the tangential velocity shows a value of 1.8 m/s, which however, is much less than the 9 m/s in the geometry 5.2. Nevertheless, the report for the total pressure drop has a value of 21.831 Pa, which is almost 1.000 Pa more than in the design 5.2.

From this analysis, it can be concluded that the pressure reduction for a four-plate grid is not as significant as the one for the eight-plate grid configuration. Nonetheless, the difference is not considerable, thereby, for the sake of simplicity, this geometry could be a feasible alternative for the design 5.2, especially that it apparently has more effect on the tangential velocity reduction.

Design 5.5

In this last design of this section, it was intended to modify the cone of the internal body in such way, that it would be transformed into a shape similar to a half-sphere, as it can be observed on the figure 81.

The figure 82 shows the scalar scene for this geometry, with the same settings as seen so far. No significant differences at the first sight can be observed with respect to the

designs 5.1 and 5.2.
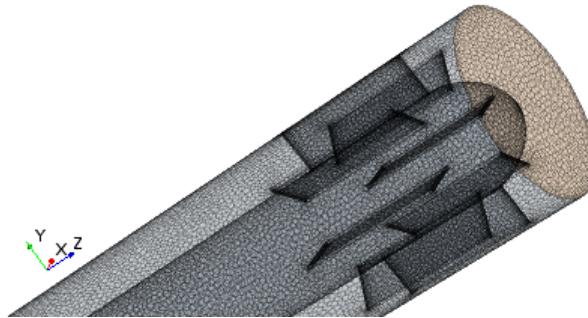
Figure 81: Design 5.5
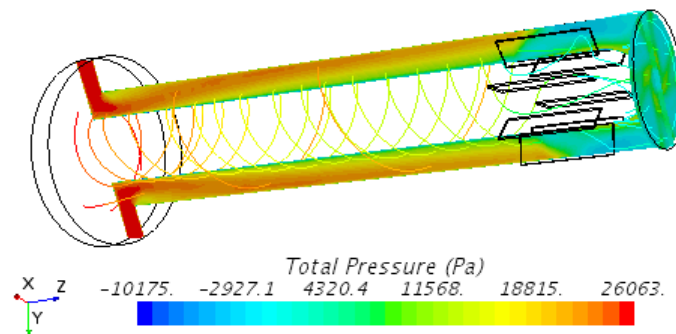
Figure 82: Scalar scene with streamlines for the design 5.5

After analyzing the plots created from the respective reports, the tangential velocity for this variable has a value of 6.13 m/s. The total pressure drop plot determines a value of 22.085 Pa, which is also more than for the first two designs of the section 5.2, which means that this approach is not very beneficial.

Design 5.6

In this design, represented on the figure 83, the internal body is a cylinder that spans throughout the entire main duct, with a height of 0,6575 m and a radius of 0,037 m, filling almost the whole duct. The grid is embedded into the internal cylinder, in form of eight plates, each with a height of 0,1 m, as it can be seen on the figure.

This way, the flow wouldn't have the pressure recirculation zones in the whole main duct, there would be no space whatsoever between the internal cylinder and the grid, and immediately upon exiting the grid, the flow would encounter the outlet. The figure 84 illustrates the scalar scene with the total pressure distribution for this case, including also the streamlines.

It can be seen that the ideas assumed in theory are indeed fulfilled. There are no recirculation zones in the duct, which was the main purpose of this approach. A detailed look at the streamlines in the grid zone is shown on the figure 85. The streamlines density has been augmented in order to illustrate more meticulously the flow's behavior in this complex region.

The figure 85 illustrates that the swirl is separated in eight segments, which breaks

it completely upon its exit. The report for the tangential velocity averaged along the circumference contained in the outlet, gives the value of 2,71 m/s. This shows that this kind of star-shaped grid is as effective in the swirl reduction as the conventional type of grid, sedulously analyzed in the chapter 4. The conclusion of this is that apparently it doesn't matter how the grid divides the swirl exactly into different segments, as long as it is altered from this natural course.
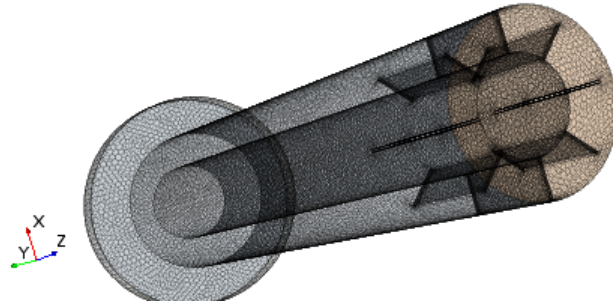
Figure 83: Design 5.6
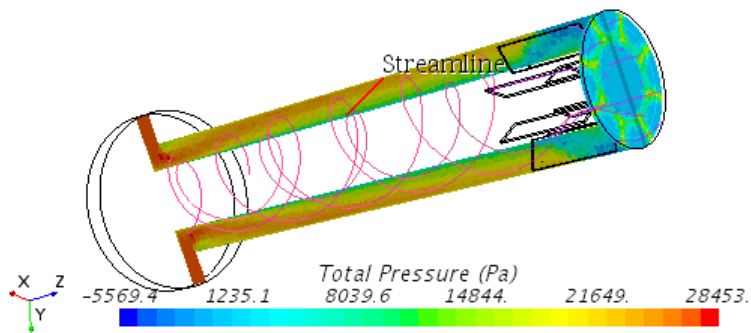
Figure 84: Scalar scene with streamlines for the design 5.6

Regarding the total pressure drop, the report shows a value of 23.007 Pa, which is almost no different from the initial geometry of this project. This shows that this approach is not comparable to the ones studied and analyzed so far, however it also eradicates the swirl movement almost completely. It can therefore be used as an alternative to the solutions studied previously, but, only in the aspect of eliminating the swirl.
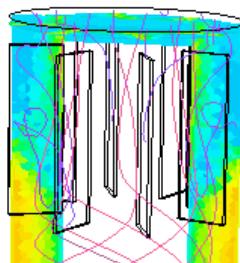
Figure 85: A detailed look at the streamlines in the grid zone for the design 5.6

It must be commented, that the first five designs of this section, did not present a

full and clear convergence of the parameters involved, even after certain simulation improvements, which makes the credibility of the results uncertain. Nevertheless, the discrepancies of the solver were not extremely high and the results turned out to be coherent. That is why they have been included in this project in order to describe their qualitative efficiency, however, taking into account the possible slight imprecision.

A summary for this section's approach is given in the table on the figure 86.

Design's number	Tangential velocity (m/s)	Static pressure drop (Pa)	Total presure drop (Pa)
5.1	-4,87	20938	20954
5.2	9	20413	20879
5.3	12,61	20596	21406
5.4	1,88	20260	21831
5.5	6,13	20216	22085
5.6	2,71	19097	23007

Figure 86: Summary of the results for the "star-shaoed" grid

It can be observed that the design 5.2 shows the best total pressure drop improvement in the section. It is more favorable than the total pressure drop for the design 4.4, which was the best design of the section 5.1 and had a total pressure drop of 21.133 Pa. It is still considerably inferior to the design 3.4 however, especially in the aspect of pressure reduction.

All the alternatives exposed in this section ended up being less propitious for this project's objectives than the geometry 5.2, however the differences in most cases are not very important, and all the designs from this section, except for the 5.3, satisfy pretty well the swirl reduction objective, which, as we must bear in mind, is by far the most important purpose of the work hereof.

A last emphasize is that, as it has been stated, the first five designs did not reach a full and clear convergence, in spite of applying several CFD pertinent tools, such as modifying the under-relaxation factors and changing the solver model to an ideal gas model. The convergence reached was imperfect, however, the imprecisions for most values were small; thereby, although the results for these five designs cannot be interpreted to the maximum degree of credibility, the conclusions obtained should still be very congruent for the project's objectives.

5.3   Turbulence induction via a set of internal tubes

The two designs of this section aim at increasing the turbulence of the flow after it has already exited the grid from the design 1.3, used as a reference in here, and after the swirl has already been drastically mitigated. The objective of this approach is to intend to reduce the pressure difference between the inlet and the outlet of the main body.

The conceptual idea is to induce turbulence by putting additional geometric elements inside the main duct, whose purpose is to alter the relatively laminar flow that exits the grid and to introduce chaotic variations inside it. The premise is that such turbulence might contribute to a smaller pressure decrease at the end of the duct.

The design 6.1 introduces two sets of cylinders perpendicular to the longitudinal axis of the main duct, and perpendicular between each other. Each of the two sets is comprised

by three, uniformly distributed small cylinders, near the outlet of the body, as it can be seen on the figure 87.
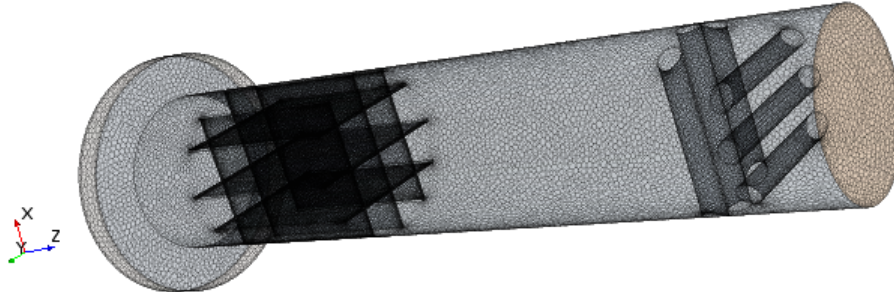
Figure 87: The design 6.1

The figure 88 shows the scalar scene for the total pressure distribution in this geometry, as well as the flow streamlines. It can be indeed observed a slight turbulence induction at the outlet by the two cylinders sets, however, it is not very significant. The tangential velocity report for the circumference created from the intersection of a cylindrical derived part of 0,057 m of diameter and the outlet, shows an averaged value of 3,25 m, which is more than the 1,53 m/s for the design 1.3. This slight variation may be caused by the fact that the chaotic movement created by the turbulence contributes to the appearance of a certain tangential component. One way or another, this difference is inconspicuous.

Regarding the total pressure drop report, this value is shown to be 22.828 Pa, considerably more than the 21.116 Pa for the design 1.3.
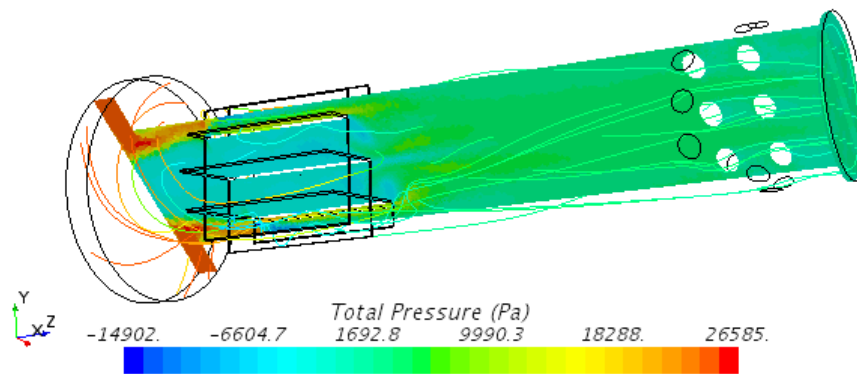
Figure 88: Scalar scene with streamlines for the design 6.1

In view of these results, this first approach for the two sets of cylinder geometry is not satisfactory.

The next design will intend to increase the turbulence induction by adding another set of uniformly distributed three cylinders, as it can be seen in detail in the figure 89.

The figure 90 shows the scalar scene with the streamlines. It can be seen how the turbulence is slightly more intense in the region of the three-set geometry. The report for the tangential velocity shows a value of 1,55 m/s, exactly the same as in the design

1.3. Notwithstanding, the total pressure drop has now increased with respect to the design 6.1, as it is now 23.810 Pa, almost 1.000 Pa more than before.
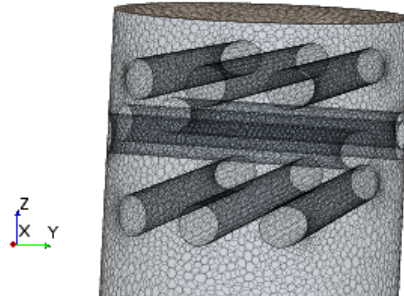
Figure 89: A detailed look at the cylinders layers from the design 6.2

The conclusion is that this path is not very promising and that further turbulence induction may not bring better results. It must be remembered that each time a geometry component is added to the flow, it creates a tiny new recirculation zone that may worsen the total pressure drop variable. This recirculation zones can be observed in the outlet of the figure 90, as thin, slightly blue lines crossing the outlet face.
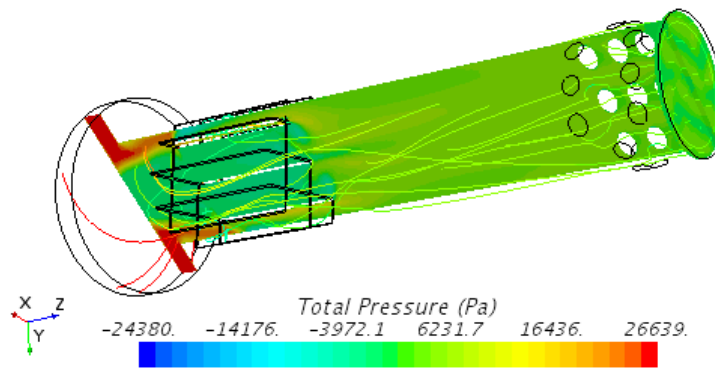
Figure 90: Scalar scene with streamlines for the design 6.2

That is why this approach will be ended in only two attempts. The exact summary is shown in the table of the figure 91.

Design's number	Tangential velocity (m/s)	Static pressure drop (Pa)	Total presure drop (Pa)
6.1	3,25	22608	22828
6.2	1,55	23209	23810

Figure 91: Summary of the designs 6.1 and 6.2

It can be observed that even the best of the two cases, the design 6.1, shows almost 2.000 Pa of difference with respect to the results without the cylinders sets, not to mention that additional geometries have additional manufacturing problems and economic costs, therefore this approach is not recommendable for this project.

5.4 The main cylinder's narrowing approach

The last of the alternative approaches proposed for this thesis, with the exceptions of those explained in the chapter 6, is aimed at narrowing the main duct right upon the air entrance to the base cylinder. When the air enters through the inlet and the swirl begins to form, the narrowing will attempt to form a drain-sort configuration that should reduce the swirl formation and thus, reduce the recirculation zone inside the swirl, at least to a certain degree. The figure 92 illustrates in detail this configuration. The fluid volume has been confined, in order to represent a solid body that was introduced inside the main duct.

The figure 93 shows the scalar scene and the streamlines for this geometry. At the first sight, it may seem as the conceptual idea has indeed been implemented with success, i.e. the swirl forms a drain configuration and afterwards passes through the grid from the design 1.3. Nevertheless, a detailed analysis shows that the simulation does not converge properly. Although the tangential velocity seems to give coherent results, 2,5 m/s, the total pressure at the inlet gives a value close to 2×10^5 Pa, which is evidently preposterous.
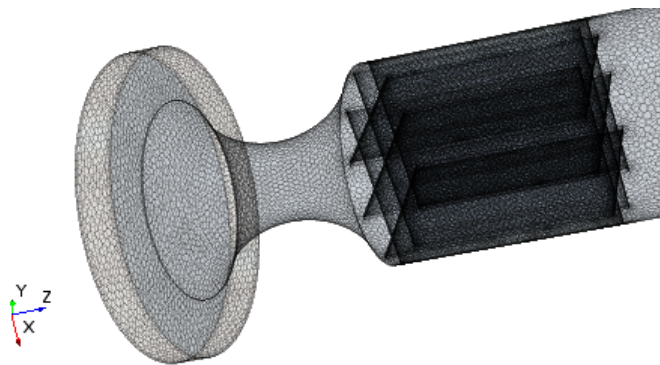
Figure 92: A detailed look at the narrowing in the duct of the design 7.1
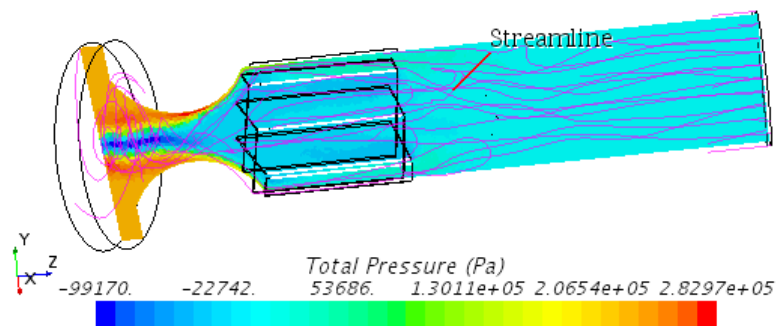
Figure 93: Scalar scene with streamlines for the design 7.1

The total pressure drop report shows a value of 186.025 Pa, which makes no sense whatsoever. Several convergence improvement tools were implemented, however, without reaching any improvement in the simulation.

Another, similar design has been tried, incrementing the distance between the narrowing and the grid, as can be appreciated on the figure 94.
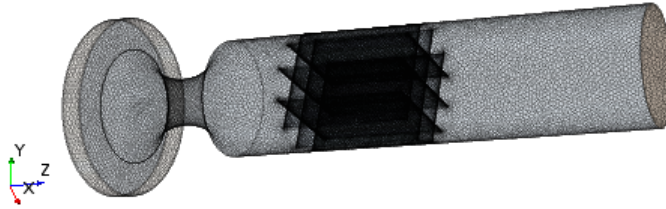
Figure 94: Scalar scene with streamlines for the design 7.1

The reports however, present exactly the same problem, the total pressure drop report gives a value of 178.450 Pa, clearly showing a simulation error, in spite of the adjustments applied.

The table on the figure 95 shows the summary for these two attempts, illustrating that the tangential velocity report may be coherent, however, the reports are definitely incoherent for all the pressure-related reports.

Design's number	Tangential velocity (m/s)	Static pressure drop (Pa)	Total presure drop (Pa)
7.1	2,5	180000	186025
7.2	3,7	170000	178450

Figure 95: Summary of the designs 7.1 and 7.2

Although the drain forming narrowing might be a reasonable conceptual approach, in this project it was not viable to perform a congruent CFD analysis of this design. This, however, may turn up to be a possible enquiry in the future projects.

Chapter 6

6 Improvement of the stator design

In the chapters 4 and 5 a detailed description of all the solutions created for the initial problem was given. The designs created had nothing whatever to do with the previous work based on the stator, however, which will be precisely the topic of the chapter 6. An attempt of improving the failed design delivered in the beginning of this thesis was carried out. Many different geometries have been tried, however, only one gave a really successful outcome.

Before proceeding to implementing the initial stator geometry, the initial design was meticulously analyzed, trying to identify its flaws and weaknesses. The figure 79 illustrates the streamlines arising from this geometry. It was concluded that a big defect of the initial stator was that it did not redirect correctly the flow, since it permitted an incontrollable escape of the flow through its lateral, open geometry. The figure 79 shows how the streamlines enter correctly the stator, however, before actually having crossed its whole body, a great part of the flow abandoned the stator completely.
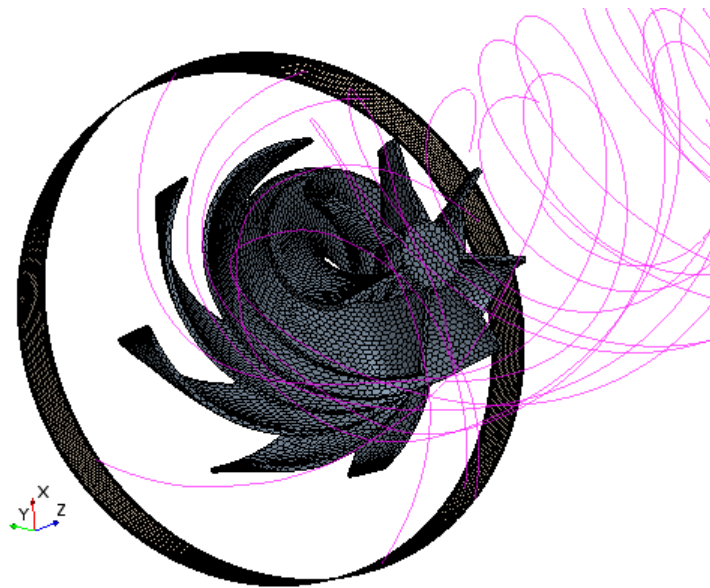
Figure 96: View of the streamlines from the initial stator geometry

It must be emphasized that the initial concept of a stator design may not be necessarily preposterous: it was the initial design from the previous work that did not accomplish its purpose. The theoretical idea of redirecting the spiral flow by a curved obstacle, that would hinder and redirect the flow's trajectory until making it laminar, could actually be really effective. The initial geometry had to be thereby improved.

6.1 Description of the design 8.1

The main problem while working with the delivered stator geometry in Star CCM+, was that the stator body was utterly contrived in a separate CAD software. That means,

that the design's parameters could not be simply altered and edited like it could have been done with a geometry constructed from the beginning. Star CCM+ allows to create all sorts of complicated geometry in its CAD option, however it is much more efficient to build them in a specific design program, such as Catia, Inventor Professional or AutoCad. That was probably the reason why the authors of the initial stator design did not perform it in StarCCM+.

The first concept for the design's improvement was to confine the streamlines inside the stator's body. A shell was built around the stator's blades, such as it can be seen in the figure 97.

Figure 97: Design 8.1 - stator enclosed by a shell

The conceptual idea was the one explained so far, the streamlines confinement would probably redirect the flow better and reduce the swirl with more effectiveness than the stator without the shell. The figure 98 illustrates the so obtained streamlines of the converged simulation.
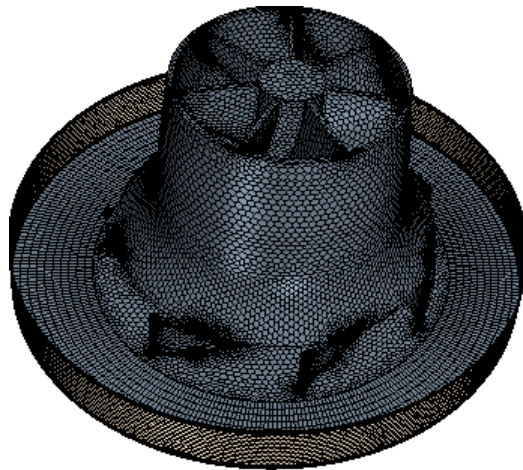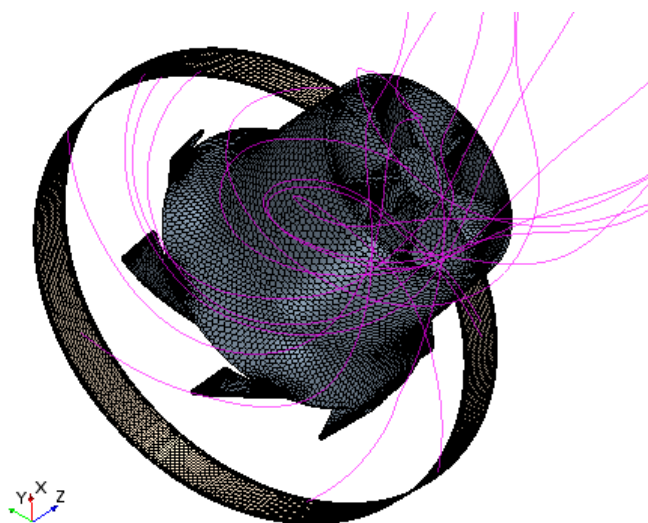

Figure 98: View of the streamlines in the design 8.1

It can be noticed how the shell indeed confines the streamlines in the flow. A perspicuous and flagrant difference can be appreciated between the streamlines in the figure 98 and 96, right upon exiting the stator. In the figure 96, the swirl is still very present, a certain reduction was indeed accomplished, however, very poorly. On the figure 98 instead, the streamlines after exiting the shell do not tend to form a swirl movement so intensely, proving that, from the visual point of view, the shell is indeed a significant improvement of the initial design.

The figure 99 shows a scalar scene of this design, with the total pressure distribution variable and with the complete view of the streamlines, right until the outlet of the whole geometry.
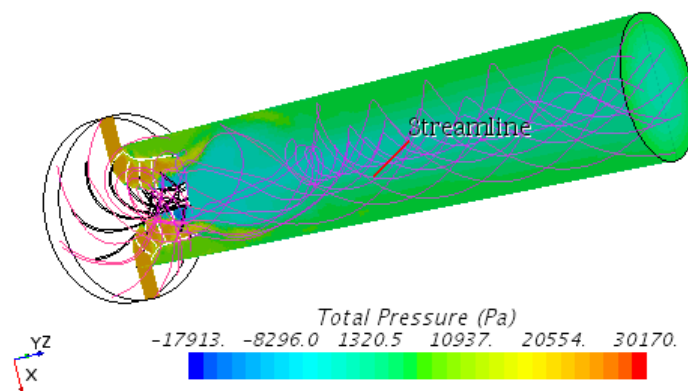

Figure 99: Scalar scene with streamlines for the design 8.1

A big improvement in the streamlines of the flow can be notices. The swirl is not eradicated, the way it was in the designs containing a grid of any kind, however it is much less pronounced than in the initial, non-stator geometry. The report for the tangential velocity, averaged along the circumference with a 0,057-meter radius, created from an intersection of a derived-part cylinder with the outlet, shows a value of 59,38 m/s. It is a considerable improvement of 32,15 per cent with respect to the non-shell stator design, that has a value of 87,52 m/s. In total, 59,38 m/s constitutes an improvement of 47,67 per cent with respect to the 113,47 m/s of the initial, non-stator geometry of the problem. Although it cannot be absolutely said that the swirl has been eradicated, it is indeed a very significant improvement of the problem's solution, which can undoubtedly constitute one of the alternative solutions for the initial geometry.

The report for the total pressure drop between the inlet and the outlet shows a value of 20.486 Pa, a slight detriment in comparison to the 20.186 Pa, which were obtained in the initial stator geometry. From an overall point of view, however, the confined stator designed shows much better results than the initial stator version.

Ideas	Tangential velocity (m/s)	Delta p (Pa)	Total pressure inlet (Pa)	Total pressure outlet (Pa)	Delta total p (Pa)
The initial geometry	113,47	18918	29498	6414	23084
The initial stator	87,52	16596	25071	4885	20186
8.1	59,38	19450	23178	2692	20486

Figure 100: Summary for the successful stator design and the comparison with both initial goemtries

The table from the figure 100 summarizes the results for the design 8.1, the design with the initial stator and the initial geometry of the problem.

It can be observed that the design 8.1, in spite of being a viable alternative, is still far inferior to absolutely all the designs containing a grid of different sorts, explained meticulously in the chapters 4 and 5.

6.2 Unsuccessful stator designs

After achieving a stator design improvement via the design 8.1, several alternatives were intended. The main concepts consisted in increasing the stator's influence upon the flow's streamlines in different ways. Nevertheless, due to the stator geometry's complexity and due to the fact that it was not created from the beginning in Star CCM+, unfortunately these designs could not deliver output results through a simulation for different reasons.

The figures 101 and 102 illustrate the first two alternative designs, which consisted in incrementing the stator blades' height, first, without any shell, and second, with a full shell covering the whole new stator.

Figure 101: An unsuccessful idea consisting in increasing the stator's height
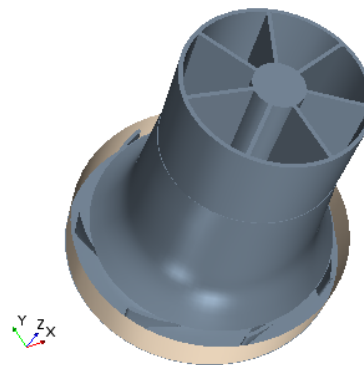
Figure 102: An unsuccessful idea consisting in increasing the stator's and the shell's height

The theoretical attempt was to prolongate the stator's effect on the flow; especially on the figure 102, the flow would probably be strongly redirected, since this geometry itself is an evident variation of the 8.1 design, to a point where it practically resembles a grid of a certain kind. Nonetheless, creating a new extrusion upon the old stator design and combining it together in Star CCM+, created an enormous amount of geometry's imperfections, that made it impossible to perform a correct meshing in these two designs.

Several tools were implemented in order to reduce the number of geometry's errors. One of them was the surface repair option of Star CCM+ software. This tool allows to identify and to fix problems of many sorts which may appear in a given geometry. The figure 103 represents a view of this tool, from the same perspective as it can be seen in the Star CCM+ software, for the geometry described on the figure 101.

As it can be seen on the figure, the number of geometry errors for this, relatively simple modification, is astounding. On the right side of the figure, a total number of 1.082
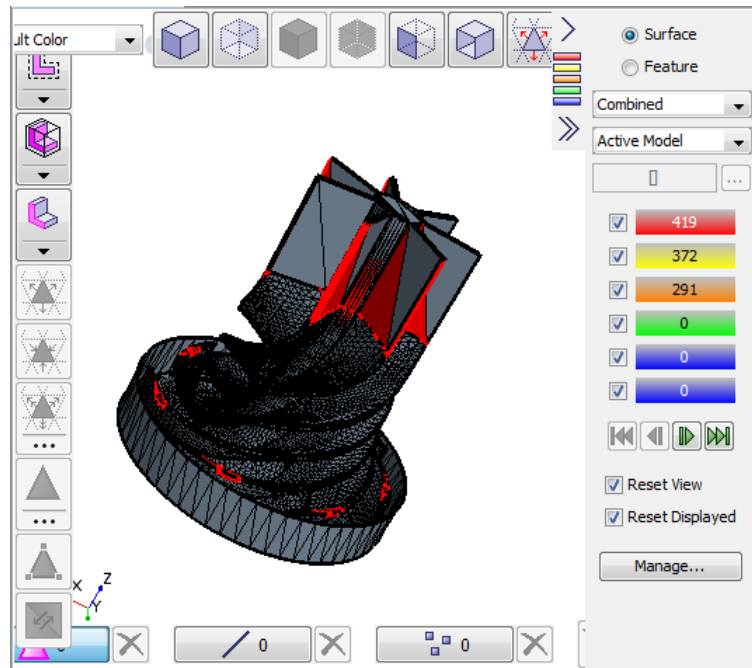
Figure 103: Surface repair tool's outcome in Star CCM+ for an unsuccessful stator geometry

different errors can be read, after being identified by the software. No matter what change was implemented, a great number of errors still appeared, and it was always too big to efficiently eliminate it via the surface repair tool.
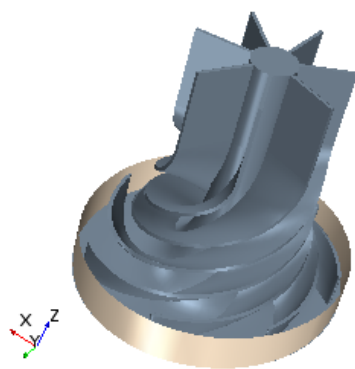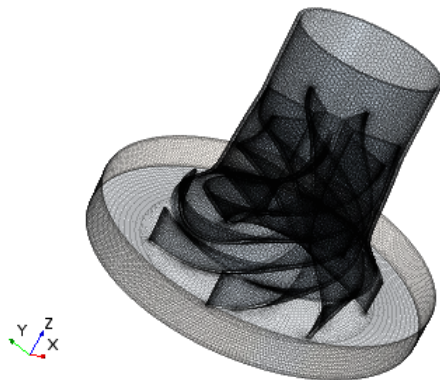

Figure 104: An unsuccessful idea consisting in increasing the shell's height
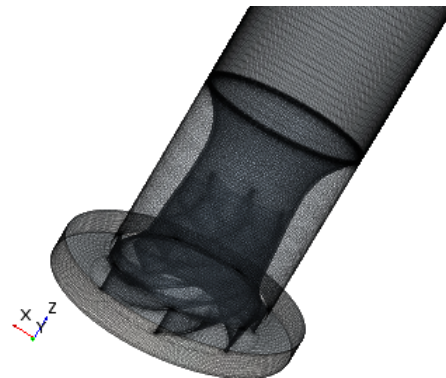
Figure 105: An unsuccessful idea consisting in increasing the shell's height and closing the recirculation zone

Different other geometries were created for the stator modification, this time without any geometry nor meshing problems, at the first sight. The figures 104 and 105 illustrate two of them. The figure 104's modification increased the height of the shell body only, creating a small cylinder inside the main duct. In the figure 105's geometry, it was intended to close the recirculation zone created with the implementation of the shell, since it enclosed the stator and this way, created a zone with very low-pressure values. This way, some total pressure drop would probably be accomplished.

Although both geometry didn't provide any meshing errors in the mesh generation stage, after being simulated by the solver, a residual divergence appeared, as it can be visualized on the figure 106.
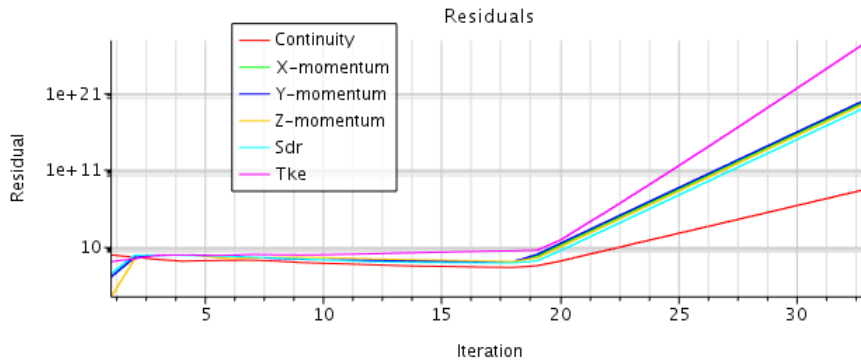
Figure 106: Residuals plot illustrating a complete divergence of the computed parameters

It can be clearly seen, that soon after initializing the case, the residuals values for all the solver equations start drastically to increase, achieving unrealistic values of the order of 10^{21}. No matter what modification was implemented, e.g. initializing the simulation from the beginning, certain geometry's improvements or customized mesh refinements, the divergence could not be resolved, making it impossible to obtain coherent results.

A last variation of the stator geometry was to combine the 8.1 design with a simple plate, such as it was seen in the chapter 4's designs. The figure 107 illustrates this geometry.
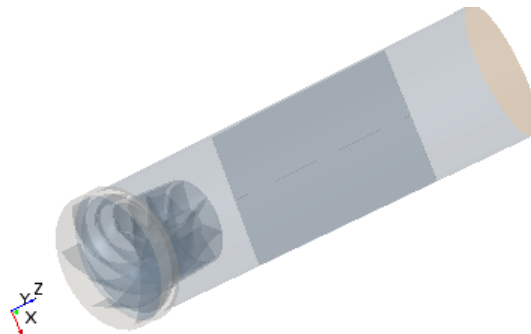
Figure 107: An unsuccessful idea consisting in adding one transversal plate to the design 8.1

Notwithstanding, this geometry also presents divergence errors in the residuals, most certainly due to an imperfect union of the plate with the main duct's external walls. The meshing in that zone was very imperfect, despite any attempts of improvement, and this design could not be finished in the development of the thesis hereof.

Chapter 7

7 Conclusions

Throughout the development of the thesis hereof, 29 different designs have been successfully implemented, in order to mitigate the problem of swirl appearance in the initially given geometry. The simulation tool used in the project was the CFD software Star CCM+. Most of the designs managed to completely eradicate the swirl, improving also the total pressure drop between the inlet and the outlet of the body.

The table from the figure 108 summarizes the best designs of each chapter.

| Design's number	Tangential velocity (m/s)	Delta p (Pa)	Total pressure inlet (Pa)	Total pressure outlet (Pa)	Delta total p (Pa)
Initial geometry	113,47	18918	29498	6414	23084
Initial stator geometry	87,52	16596	25071	4885	20186
3.4 (Chapter 4.6)	1,8	19151	20613	1430	19183
4.4 (Chapter 5.1)	3,36	21071	22627	1494	21133
5.2 (Chapter 5.2)	3,8	20523	22701	1975	20726
8.1 (Chapter 6)	59,38	19450	23178	2692	20486

Figure 108: The summary of the most successfull designs of each chapter

It has been made utterly clear in the chapter 4.6 that the optimum design of all is the geometry 3.4. Not only does it manage to accomplish a 98,41 per cent reduction in the tangential velocity upon the reference derived part, but also it achieves an improvement of the total pressure drop in 16,89 per cent, with respect to the initial geometry of the problem.

This geometry, consisting in a correctly configured and located grid inside the main duct, has been selected from a meticulous parametric study of the grid's plate number, its optimum location and the ideal plates' height. Another considerable advantage of this geometry over all the other alternatives, is its relative simplicity in the manufacturing. This way, the time and the manufacturing work, as well as the related costs, which are the preponderant factors in any industrial application, can be optimized. The figure 109, which is the repetition of the figure 54, illustrates once more this optimal design.
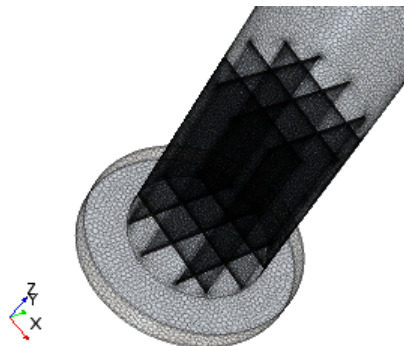

Figure 109: The design 3.4, the optimum design both from the swirl reduction and from the total pressure drop reduction points of view

The summary for the grid's correct characteristics, deduced from the simulations performed, is the following one. In the first place, the grid ought to be comprised by the biggest number of plates as possible, taking into consideration that the manufacturing complexity increases along with the number. In the second place, the grid should be located as low as possible. Finally, as a general rule, the grid's height should be incremented to a certain limit explained in the chapter 4.5.

The recirculation zones-filling designs, from which the optimum concept turned out to be the design 4.4, proved to be effective in the pressure drop reduction only to a certain extent, definitely not more than the design 3.4. They also must include the grid anyway, in order to reduce the swirl flow, which overall, makes them much more complex to manufacture than the grid alone.

The "star-shaped" grid designs, from which the best turned out to be the geometry 5.2, provide an interesting alternative, however inferior, to the 3.4 geometry. The theoretical concept of turbulence induction, attempted in the chapter 5.3, proved not to bring any qualitative improvements of any sort, at least in the way implemented in this project.

Finally, a considerable improvement of the initial stator geometry was accomplished via the design 8.1, which confined the stator within a shell. It reduced the tangential velocity at the reference derived part in 32,15 per cent with respect to the initial stator, suffering however a slight, yet little significant detriment in the total pressure aspect. Nonetheless, this type of geometry proved to be far inferior than any of the beforementioned ones, in addition of being much more complex to manufacture.

A quick review of the failed designs, as well as the possible propositions for the future, shall be exposed in the next chapter.

Chapter 8

8 Future approaches

Regarding the main purpose of this thesis, as it has been clarified in the previous chapter, there is no real need to focus on the swirl reduction aspect anymore, since the swirl has been eradicated in a lot of different ways. Notwithstanding, the total pressure drop between the inlet and the outlet, however improved, can still be probably reduced to some extent. This is precisely what future projects in this field may attempt at.

Pertaining to the designs of this project, there have been two design concepts that ended up being unsuccessful. The first failed theoretical idea was described in the chapter 5.4, and aimed at narrowing the main duct right upon the air entrance to the base cylinder, such as it is once again shown on the figure 110. The initial attempt was to form a drain-sort configuration that might reduce the swirl formation and thus, reduce the recirculation zone inside the swirl. Nevertheless. The design's results were incoherent, probably due to an improper convergence, and despite the corrections tried, no improvement was achieved. It would be interesting to intend this concept in other ways, until obtaining appropriate results, and to conclude whether or not it actually helps improve the pressure drop.
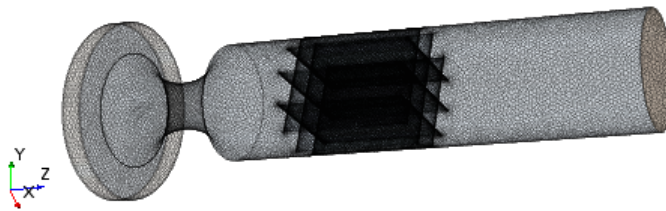
Figure 110: The design 7.1, the unsuccessful design aimed at narrowing the main duct. Its CFD results in this project were preposterous, despite the corrections applied.

The second unsuccessful concept was the set of stator-improving ideas implemented and described in the chapter 6.2. Several different geometries were intended, e.g. incrementing the stator's height, incrementing the shell's height or adding a plate to the duct. As it was described in the chapter 6.2, despite all the corrections to the simulations, different sorts of meshing and divergence errors hindered the process. The stator-related designs, although much more complex than the original geometries created in this project, may still bring some pertinent improvements to the pressure drop in the future.

Chapter 9

9 Project's budget

This chapter is a summary of the economic costs that have been necessary in order to fulfill the development of this document. In the first place, a description of each project's phase shall be given. Afterwards, a detailed analysis of the costs related to these stages will be presented and, finally, a global summary of the costs will be exposed.

9.1 Project's phases description

The project's development from the beginning until finishing this document can be depicted in six phases:

Phase I – Theoretical preparation via Star CCM+ tutorials study: before commencing the actual work process, a sedulous analysis of 28 CFD software tutorials had been carried out, covering over 700 pages describing the different Star CCM+ tools. This study allowed the author to acquire the appropriate level of knowledge that made possible the execution of this project.

Phase II - Initial geometries analysis: in this phase, all the tasks related to the study of the initially provided designs have been taken into account. Since the whole preprocess and the solver had been previously configured, the only aspect carried out in here was the CFD postprocess analysis and understanding of the two basic designs.

Phase III - New geometries design and meshing: this phase involves all the work linked to the creation of the original geometries explained in this document, and to the finishing the meshing of all these designs. The mesh independence study is also included in this phase.

Phase IV – Simulations configurations and solver: in here all the steps pertinent to the physical models setting, as well as the setting of the boundary conditions have been summarized from the economic point of view. This phase includes also the time invested in the actual CFD computations by the solver.

Phase V – Postprocess analysis: all the aspects apposite to the solvers' results analysis have been included. This involved the creation of all the necessary tables, plots and diagrams that enabled to visualize all the important information obtained.

Phase VI - Document's preparation: the final phase included the preparation of the document hereof, including the bibliography revision, the implementation in Latex software, as well as the time invested in the correction of the document by the tutor engineering in charge.

9.2 Partial costs

The table from the figure 111 illustrates the detailed description of the costs pertaining to each of the six stages of the project.

Phase number	Components description	Time (h)	Costs per hour (€/h)	Costs (€)
I	Engineer	70	40	2.800
	PhD tutor engineer	12	60	720
	Auxiliary CFD experts	8	40	320
	Licenses	70	5	350
				Total: 4.190
II	Engineer	6	40	240
	PhD tutor engineer	2	60	120
	Auxiliary CFD experts	1	40	40
	Licenses	6	5	30
				Total: 430
III	Engineer	25	40	1.000
	PhD tutor engineer	8	60	480
	Auxiliary CFD experts	7	40	280
	Licenses	15	5	75
				Total: 1.835
IV	Engineer	7	40	280
	PhD tutor engineer	3	60	180
	Auxiliary CFD experts	1	40	40
	Licenses	40	5	200
				Total: 700
V	Engineer	12	40	480
	PhD tutor engineer	3	60	180
	Auxiliary CFD experts	2	40	80
	Licenses	12	5	60
				Total: 800
VI	Engineer	75	40	3.000
	PhD tutor engineer	10	60	600
				Total: 3.600

Figure 111: The summary of the costs concerning each of the six project's phases

The table from the figure 112 illustrates the costs of the hardware indispensable for the performance of this project.

Hardware component	Total cost (€)
Workstation	4.000
Laptop computer	800

Figure 112: The summary of the costs concerning the hardware

9.3 Global costs

Finally, the table from the figure 113 shows the summary of the total costs:

Description	Total costs (€)
Phase I	4.190
Phase II	430
Phase III	1.835
Phase IV	700
Phase V	800
Phase VI	3.600
Hardware components	4.800
Total:	**16.355**

Figure 113: The summary of overall project's costs

After taking into consideration all the relevant elements of the project, the overall cost of its execution turned out to be:

Sixteen thousand three hundred and fifty-five euros

Chapter 10

10 Bibliography

[1] Antonio Gil Megías **Modelado tridimensional del flujo de aire en el cilindro de motores Diesel de inyección directa.** Editorial Reverté. CMT - Motores Térmicos UPV.

[2] M.B. Abbot and D.R. Basco **Computational Fluid Dynamics. An introduction for engineers.** Longman Singapore Publishers Ltd. 1989.

[3] J.D. Anderson Jr. **Computational Fluid Dynamics. The basis with applications.** Mcgraw-Hill Inc. 1995.

[4] J.D. Anderson Jr. **Fundamentals of Aerodynamics.** Mcgraw-Hill Series in Aeronautical and Aerospace Engineering. 2005.

[5] R. Cebeci, J.P. Shao, F. Kafyeke **Computational Fluid Dynamics for engineers.** Springer Berlin Haidelberg. 2005.

[6] D.C. Wilcox **Turbulence Modeling for CFD.** DCW Industries, La Canada (California). 1998.

[7] John B. Heywood **Internal Combustion Engines Fundamentals.** McGraw-Hill Inc. Massachusetts Institute of Technology. 1998.

[8] F. Payri, J.M. Desantes **Motores de combustión interna alternativos.** Editorial Reverté and Editorial UPV. 2011.

[9] Milovan Peric, Stephen Ferguson **The advantage of polyhedral meshes.** CD-Adapco.

[10] Robert Eymard, Thierry Gallouet and Raphaele Herbin **Finite Volume Methods.** January 2003.

[11] **Star CCM+ User's Guide** CD-Adapco. 2014.

[12] G. Tippelman **A new method of investigation of swirl ports.** SAE Paper 770404. 1977.

[13] P. Moin and J. Kim **Simulación de la turbulencia mediante superordenadores.** Investigación y docencia. 1997.

[14] https://www.cfd-online.com/Wiki/SST k-omega model

[15] https://www.sharcnet.ca/Software/Fluent6/html/ug/node987.htm

[16] http://www.cfdyna.com/Notes/Solution/Segregated.pdf

[17] http://www.engineering.com/DesignSoftware/DesignSoftwareArticles/ArticleID/9296/3-Criteria-for-Assessing-CFD-Convergence.aspx

[18] http://nht.xjtu.edu.cn/paper/en/2007219.pdf